











TECH BRIEFS

NATIONAL AERONAUTICS AND SPACE ADMINISTRATION

-  Technology Focus
-  Electronics/Computers
-  Software
-  Materials
-  Mechanics/Machinery
-  Manufacturing
-  Bio-Medical
-  Physical Sciences
-  Information Sciences
-  Books and Reports

INTRODUCTION

Tech Briefs are short announcements of innovations originating from research and development activities of the National Aeronautics and Space Administration. They emphasize information considered likely to be transferable across industrial, regional, or disciplinary lines and are issued to encourage commercial application.

Availability of NASA Tech Briefs and TSPs

Requests for individual Tech Briefs or for Technical Support Packages (TSPs) announced herein should be addressed to

National Technology Transfer Center

Telephone No. **(800) 678-6882** or via World Wide Web at <http://www.nttc.edu/about/contactus.asp>

Please reference the control numbers appearing at the end of each Tech Brief. Information on NASA's Innovative Partnerships Program (IPP), its documents, and services is also available at the same facility or on the World Wide Web at <http://ipp.nasa.gov>.

Innovative Partnerships Offices are located at NASA field centers to provide technology-transfer access to industrial users. Inquiries can be made by contacting NASA field centers listed below.

NASA Field Centers and Program Offices

Ames Research Center
Lisa L. Lockyer
(650) 604-1754
lisa.l.lockyer@nasa.gov

Dryden Flight Research Center
Gregory Poteat
(661) 276-3872
greg.poteat@dfrc.nasa.gov

Glenn Research Center
Kathy Needham
(216) 433-2802
kathleen.k.needham@nasa.gov

Goddard Space Flight Center
Nona Cheeks
(301) 286-5810
nona.k.cheeks@nasa.gov

Jet Propulsion Laboratory
Ken Wolfenbarger
(818) 354-3821
james.k.wolfenbarger@jpl.nasa.gov

Johnson Space Center
Michele Brekke
(281) 483-4614
michele.a.brekke@nasa.gov

Kennedy Space Center
David R. Makufka
(321) 867-6227
david.r.makufka@nasa.gov

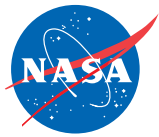
Langley Research Center
Martin Waszak
(757) 864-4015
martin.r.waszak@nasa.gov

Marshall Space Flight Center
Jim Dowdy
(256) 544-7604
jim.dowdy@msfc.nasa.gov

Stennis Space Center
John Bailey
(228) 688-1660
john.w.bailey@nasa.gov

Carl Ray, Program Executive
Small Business Innovation
Research (SBIR) & Small
Business Technology
Transfer (STTR) Programs
(202) 358-4652
carl.g.ray@nasa.gov

Doug Comstock, Director
Innovative Partnerships
Program Office
(202) 358-2560
doug.comstock@nasa.gov



TECH BRIEFS

NATIONAL AERONAUTICS AND SPACE ADMINISTRATION



5 Technology Focus: Test & Measurements

- 5 Digital Phase Meter for a Laser Heterodyne Interferometer
- 6 Vision System Measures Motions of Robot and External Objects
- 6 Advanced Precipitation Radar Antenna To Measure Rainfall From Space
- 7 Wide-Band Radar for Measuring Thickness of Sea Ice
- 8 Vertical Isolation for Photodiodes in CMOS Imagers
- 9 Wide-Band Microwave Receivers Using Photonic Processing



11 Electronics/Computers

- 11 L-Band Transmit/Receive Module for Phase-Stable Array Antennas
- 11 Microwave Power Combiner/Switch Utilizing a Faraday Rotator
- 12 Compact Low-Loss Planar Magic-T
- 12 Using Pipelined XNOR Logic to Reduce SEU Risks in State Machines
- 13 Quasi-Optical Transmission Line for 94-GHz Radar
- 13 Next Generation Flight Controller Trainer System



15 Software

- 15 Converting From DDOR SASF to APF
- 15 Converting From CVF to AAF
- 15 Documenting AUTOGEN and APGEN Model Files
- 15 Sequence History Update Tool
- 15 Extraction and Analysis of Display Data
- 16 MRO DKF Post-Processing Tool
- 16 Rig Diagnostic Tools
- 16 MRO Sequence Checking Tool
- 16 Science Activity Planner for the MER Mission
- 16 UAVSAR Flight-Planning System



19 Manufacturing & Prototyping

- 19 Templates for Deposition of Microscopic Pointed Structures



21 Materials

- 21 Adjustable Membrane Mirrors Incorporating G-Elastomers
- 21 Hall-Effect Thruster Utilizing Bismuth as Propellant
- 21 High-Temperature Crystal-Growth Cartridge Tubes Made by VPS
- 22 Quench Crucibles Reinforced With Metal



23 Mechanics/Machinery

- 23 Deep-Sea Hydrothermal-Vent Sampler
- 24 Mars Rocket Propulsion System
- 24 Two-Stage Passive Vibration Isolator
- 24 Improved Thermal Design of a Compression Mold
- 25 Enhanced Pseudo-Waypoint Guidance for Spacecraft Maneuvers



27 Physical Science

- 27 Altimetry Using GPS-Reflection/Occultation Interferometry
- 27 Thermally Driven Josephson Effect
- 27 Perturbation Effects on a Supercritical C_7H_{16}/N_2 Mixing Layer
- 28 Gold Nanoparticle Labels Amplify Ellipsometric Signals
- 28 Phase Matching of Diverse Modes in a WGM Resonator
- 29 WGM Resonators for Terahertz-to-Optical Frequency Conversion
- 30 Determining Concentration of Nanoparticles From Ellipsometry
- 31 Microwave-to-Optical Conversion in WGM Resonators
- 31 Four-Pass Coupler for Laser-Diode-Pumped Solid-State Laser
- 32 Low-Resolution Raman-Spectroscopy Combustion Thermometry
- 34 Temperature Sensors Based on WGM Optical Resonators
- 35 Varying the Divergence of Multiple Parallel Laser Beams



37 Information Sciences

- 37 Efficient Algorithm for Rectangular Spiral Search
- 37 Algorithm-Based Fault Tolerance Integrated With Replication
- 38 Targeting and Localization for Mars Rover Operations
- 38 Terrain-Adaptive Navigation Architecture
- 38 Self-Adjusting Hash Tables for Embedded Flight Applications
- 39 Schema for Spacecraft-Command Dictionary



41 Books & Reports

- 41 Combined GMSK Communications and PN Ranging
- 41 System-Level Integration of Mass Memory
- 41 Network-Attached Solid-State Recorder Architecture
- 41 Method of Cross-Linking Aerogels Using a One-Pot Reaction Scheme
- 41 An Efficient Reachability Analysis Algorithm

This document was prepared under the sponsorship of the National Aeronautics and Space Administration. Neither the United States Government nor any person acting on behalf of the United States Government assumes any liability resulting from the use of the information contained in this document, or warrants that such use will be free from privately owned rights.



Digital Phase Meter for a Laser Heterodyne Interferometer

The design is suitable for numerous commercial products that utilize phase measurements.

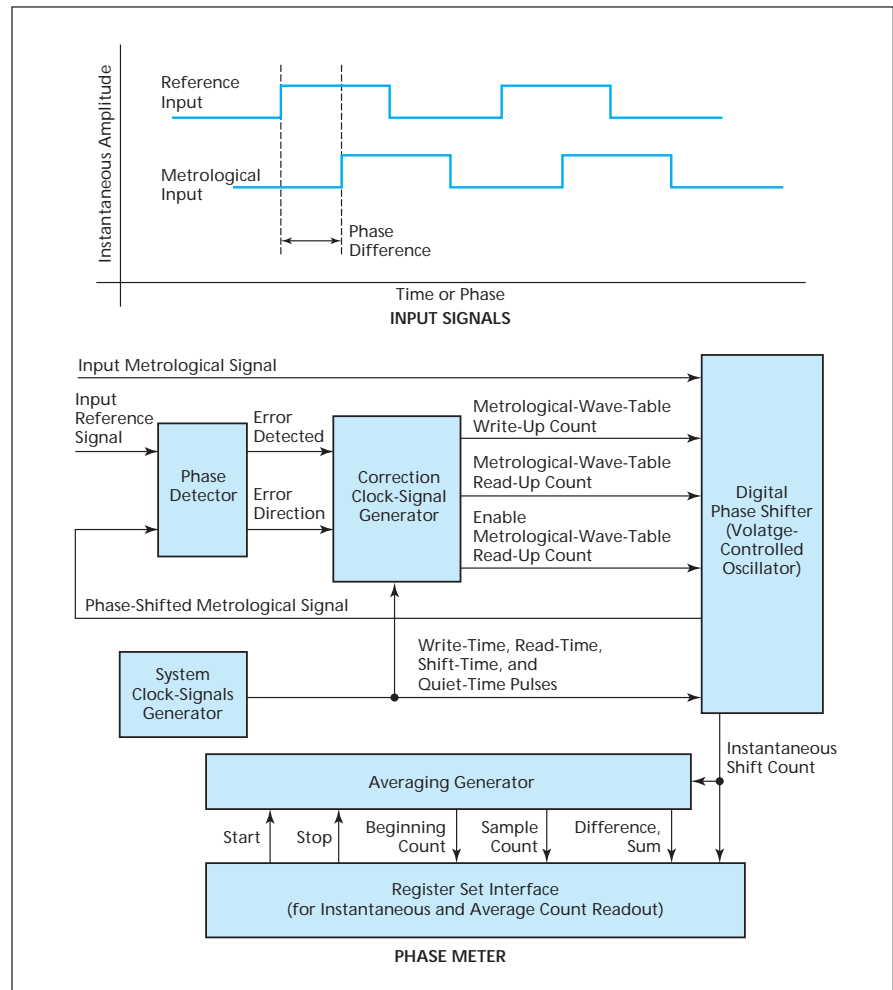
NASA's Jet Propulsion Laboratory, Pasadena, California

The figure depicts two digital waveforms and a block diagram of a digital phase meter for measuring the difference between their phases. This digital phase meter is being developed for incorporation into a laser heterodyne interferometer in a metrological apparatus, but could also be adapted to other uses. Relative to prior phase meters of similar capability, including digital ones, this digital phase meter is smaller, less complex, and less expensive. The phase meter has been constructed and tested in the form of a field-programmable gate array (FPGA) of fewer than 10^4 gates.

A description of the signals to be processed is prerequisite to a meaningful description of this digital phase meter. There are two digital, half-duty-cycle square-wave input signals, denoted the reference and metrological input, respectively. Both signals oscillate at the same frequency, which, in the original intended application, is the laser heterodyne frequency (typically of the order of 100 kHz). In the original intended application, the phase difference between the two signals is directly proportional to a relative change in the lengths of portions of an optical path traversed by the laser beam.

The three main components at the heart of the phase meter are a phase detector, a correction clock-signal generator, and a digital phase shifter. These components are connected to form a phase-locked loop (PLL) that is a slightly modified version of a conventional PLL. The modification consists mainly in feeding the metrological input signal, instead of the reference input signal, to one of the input terminals of the phase shifter. That is to say, whereas the phase of the reference signal gets shifted in a conventional PLL, the phase of the metrological signal is the one that gets shifted in this PLL.

The reference signal is fed to one of the two inputs of a phase detector, while the phase-shifted metrological signal is fed to the other input of the phase detector, which measures the difference between the phases of its inputs and puts out a correction command (basically, a



The Digital Phase Meter is based on a modified phase-locked loop. When phase alignment between the reference input and the phase-shifted metrological input is achieved, the loop locks and the phase shift of the digital phase shifter equals the phase difference that one seeks to measure.

pair of error feedback signals) in an effort to drive the difference toward zero. The correction command is fed to the correction clock-signal generator, the outputs of which are fed as inputs to the digital phase shifter. The overall action of the loop is to shift the phase of the metrological signal until it becomes phase-aligned with the reference signal. When this alignment is achieved, the phase detector stops sending correction commands to the phase shifter.

One of the outputs of the phase detector is a number proportional to the in-

stantaneous phase shift imposed on the metrological signal. This number is fed to an averaging generator and a register set interface for display of instantaneous and time-averaged phase readings, which can include readings from which initial values have been subtracted so as to indicate the change in phase shift from the initial to the current or final state of a metrological process.

This work was done by Frank Loya of Caltech for NASA's Jet Propulsion Laboratory. Further information is contained in a TSP (see page 1). NPO-40318

Vision System Measures Motions of Robot and External Objects

Frame rates greatly exceed those of prior systems.

NASA's Jet Propulsion Laboratory, Pasadena, California

A prototype of an advanced robotic vision system both (1) measures its own motion with respect to a stationary background and (2) detects other moving objects and estimates their motions, all by use of visual cues. Like some prior robotic and other optoelectronic vision systems, this system is based partly on concepts of optical flow and visual odometry. Whereas prior optoelectronic visual-odometry systems have been limited to frame rates of no more than 1 Hz, a visual-odometry subsystem that is part of this system operates at a frame rate of 60 to 200 Hz, given optical-flow estimates. The overall system operates at an effective frame rate of 12 Hz. Moreover, unlike prior machine-vision systems for detecting motions of external objects, this system need not remain stationary: it can detect such motions while it is moving (even vibrating).

The system includes a stereoscopic pair of cameras mounted on a moving robot. The outputs of the cameras are digitized, then processed to extract positions and velocities. The initial image-data-processing functions of this system are the same as those of some prior systems: Stereoscopia is used to compute three-dimensional (3D) positions for all pixels in the camera images. For each pixel of each image, optical flow between successive image frames is used to compute the two-

dimensional (2D) apparent relative translational motion of the point transverse to the line of sight of the camera.

The challenge in designing this system was to provide for utilization of the 3D information from stereoscopia in conjunction with the 2D information from optical flow to distinguish between motion of the camera pair and motions of external objects, compute the motion of the camera pair in all six degrees of translational and rotational freedom, and robustly estimate the motions of external objects, all in real time. To meet this challenge, the system is designed to perform the following image-data-processing functions:

The visual-odometry subsystem (the subsystem that estimates the motion of the camera pair relative to the stationary background) utilizes the 3D information from stereoscopia and the 2D information from optical flow. It computes the relationship between the 3D and 2D motions and uses a least-mean-squares technique to estimate motion parameters. The least-mean-squares technique is suitable for real-time implementation when the number of external-moving-object pixels is smaller than the number of stationary-background pixels.

In another subsystem, pixels representative of external transversely moving objects are detected by means of differ-

ences between (1) apparent transverse velocities computed from optical flow and (2) the corresponding relative transverse velocities estimated from visual odometry under the temporary assumption that all pixels belong to the stationary background.

In yet another subsystem, pixels representative of radially moving objects are detected by means of differences between (1) changes in radial distance estimated from changes in stereoscopic disparities between successive image frames and (2) the corresponding relative radial velocities estimated from visual odometry under the temporary assumption that all pixels belong to the stationary background. However, it is more difficult to detect radial than to detect transverse motion, especially at large distances. This difficulty is addressed by incorporating several additional processing features, including means to estimate rates of change of stereoscopic disparities, post-processing to prevent false alarms at low signal-to-noise ratios, and taking advantage of sometimes being able to distinguish between radial-motion optical flow and transverse-motion optical flow at short distances.

This work was done by Ashit Talukder and Larry Matthies of Caltech for NASA's Jet Propulsion Laboratory. Further information is contained in a TSP (see page 1). NPO-40687

Advanced Precipitation Radar Antenna To Measure Rainfall From Space

This parabolic cylindrical reflector uses Ku and Ka bands.

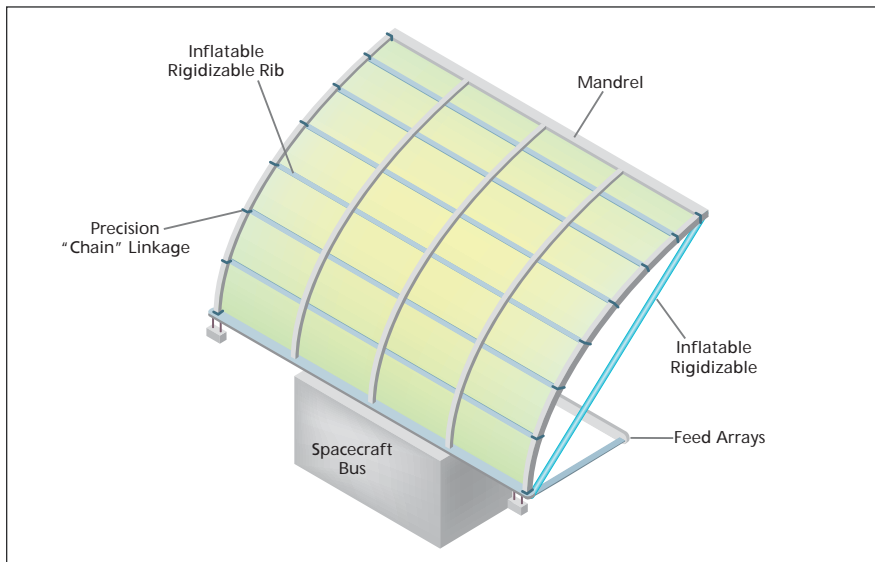
NASA's Jet Propulsion Laboratory, Pasadena, California

To support NASA's planned 20-year mission to provide sustained global precipitation measurement (EOS-9 Global Precipitation Measurement (GPM)), a deployable antenna has been explored with an inflatable thin-membrane structure. This design uses a 5.3×5.3-m inflatable parabolic reflector with the electronically scanned, dual-frequency phased array feeds to provide improved rainfall measurements at 2.0-km horizontal resolution over a cross-track scan range of up to ±37°, necessary for resolving intense,

isolated storm cells and for reducing the beam-filling and spatial sampling errors. The two matched radar beams at the two frequencies (Ku and Ka bands) will allow unambiguous retrieval of the parameters in raindrop size distribution.

The antenna is inflatable, using rigidizable booms, deployable chain-link supports with prescribed curvatures, a smooth, thin-membrane reflecting surface, and an offset feed technique to achieve the precision surface tolerance (0.2 mm RMS) for meet-

ing the low-sidelobe requirement. The cylindrical parabolic offset-feed reflector augmented with two linear phased array feeds achieves dual-frequency shared-aperture with wide-angle beam scanning and very low sidelobe level of -30 dB. Very long Ku and Ka band microstrip feed arrays incorporating a combination of parallel and series power divider lines with cosine-overpedestal distribution also augment the sidelobe level and beam scan. This design reduces antenna mass and launch



The configuration of the radar antenna features a Chain-Link Support Structure that is space-deployable.

vehicle stowage volume. The Ku and Ka band feed arrays are needed to achieve the required cross-track beam scanning. To demonstrate the inflatable cylindrical reflector with two linear polarizations (V and H), and two beam directions (0° and 30°), each frequency band has four individual microstrip

array designs. The Ku-band array has a total of 166×2 elements and the Ka-band has 166×4 elements with both bands having element spacing about $0.65 \lambda_0$.

The cylindrical reflector with offset linear array feeds reduces the complexity from "N×N" transmit/receive (T/R)

modules of a conventional planar-phased array to just "N" T/R modules. The antenna uses T/R modules with electronic phase-shifters for beam steering. The offset reflector does not provide poor cross-polarization like a double-curved offset reflector would, and it allows the wide scan angle in one plane required by the mission. Also, the cylindrical reflector with two linear array feeds provides dual-frequency performance with a single, shared aperture. The aperture comprises a reflective surface with a focal length of 1.89 m and is made from aluminized Kapton film. The reflective surface is of uniform thickness in the range of a few thousandths of an inch and is attached to the chain-link support structure via an adjustable suspension system. The film aperture rolls up, together with the chain-link structure, for launch and can be deployed in space by the deployment of the chain-link structure.

This work was done by Yahya Rahmat-Samii of UCLA; John Lin of ILC Dover, Inc.; and John Huang, Eastwood Im, Michael Lou, Bernardo Lopez, and Stephen Durden of Caltech for NASA's Jet Propulsion Laboratory. For more information, contact iaoffice@jpl.nasa.gov. NPO-40470

Wide-Band Radar for Measuring Thickness of Sea Ice

This instrument could contribute to understanding of climate change.

NASA's Jet Propulsion Laboratory, Pasadena, California

A wide-band penetrating radar system for measuring the thickness of sea ice is under development. The need for this or a similar system arises as follows: Spatial and temporal variations in the thickness of sea ice are important indicators of heat fluxes between the ocean and atmosphere and, hence, are important indicators of climate change in polar regions. A remote-sensing system that could directly measure the thickness of sea ice over a wide thickness range from aboard an aircraft or satellite would be of great scientific value. Obtaining thickness measurements over a wide region at weekly or monthly time intervals would contribute significantly to understanding of changes in the spatial distribution and of the mass balance of sea ice.

A prototype of the system was designed on the basis of computational simulations directed toward understanding what signal frequencies are

needed to satisfy partly competing requirements to detect both bottom and top ice surfaces, obtain adequate penetration despite high attenuation in the lossy sea-ice medium, and obtain adequate resolution, all over a wide thickness range. The prototype of the system is of the frequency-modulation, continuous-wave (FM-CW) type. At a given time, the prototype functions in either of two frequency-band/operational-mode combinations that correspond to two thickness ranges: a lower-frequency (50 to 250 MHz) mode for measuring thickness greater than about 1 m, and a higher-frequency (300 to 1,300 MHz) mode for measuring thickness less than about 1 m. The bandwidth in the higher-frequency (lesser-thickness) mode is adequate for a thickness resolution of 15 cm; the bandwidth in the lower-frequency (greater-thickness) mode is adequate for a thickness resolution of 75

cm. Although a thickness resolution of no more than 25 cm is desired for scientific purposes, the 75-cm resolution was deemed acceptable for the purpose of demonstrating feasibility.

The prototype was constructed as a modified version of a 500-to-2,000-MHz FM-CW radar system developed previously for mapping near-surface internal layers of the Greenland ice sheet. The prototype included two sets of antennas: one for each frequency-band/mode. For Arctic and Antarctic field tests, the prototype was mounted on a sled that was towed across the ice. The Arctic field test was performed in the lower-frequency mode on ice ranging in thickness from 1 to 4 m. In the analysis of the results of the Arctic field test, a comparison of the radar-determined ice thicknesses with actual ice thicknesses yielded an overall mean difference of 14 cm and standard deviation of 30 cm. The Antarctic field test was performed in the higher-fre-

quency mode; analysis of the results led to the conclusion that this mode is useful for measuring thicknesses between 0.5 and 1 m.

Several modifications have been conceived for implementation in further development toward an improved practical system:

- The system would function in a single frequency-band/mode (100 to 1,200 MHz) that would afford a resolution of about 15 cm.

- There would be a single antenna system that would be optimized for the entire 100-to-1,000-MHz frequency band.
- To enable ice-thickness surveys over larger areas, the system would be made capable of operating aboard a low-flying aircraft that could be either piloted or robotic.
- Data-processing techniques to deconvolve the system response have been developed on the basis of impulse-re-

sponse measurements over a calm ocean. Implementation of these techniques in the system would enable correction for imperfections of the system and would thereby increase the effective sensitivity of the system.

This work was done by Prasad Gogineni and Pannir Kanagaratnam of the University of Kansas and Benjamin M. Holt of Caltech for NASA's Jet Propulsion Laboratory. Further information is contained in a TSP (see page 1). NPO-45565

Vertical Isolation for Photodiodes in CMOS Imagers

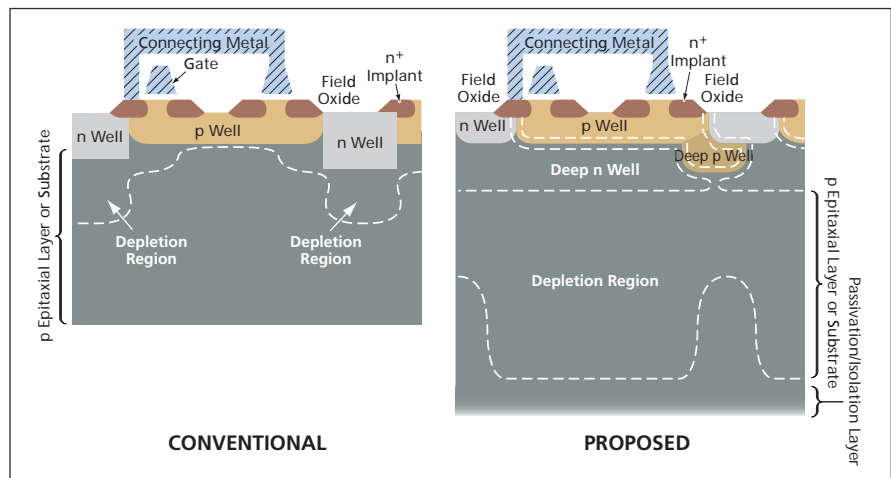
Diffusion cross-talk would be reduced substantially.

NASA's Jet Propulsion Laboratory, Pasadena, California

In a proposed improvement in complementary metal oxide/semiconductor (CMOS) image detectors, two additional implants in each pixel would effect vertical isolation between the metal oxide/semiconductor field-effect transistors (MOSFETs) and the photodiode of the pixel. This improvement is expected to enable separate optimization of the designs of the photodiode and the MOSFETs so as to optimize their performances independently of each other. The purpose to be served by enabling this separate optimization is to eliminate or vastly reduce diffusion cross-talk, thereby increasing sensitivity, effective spatial resolution, and color fidelity while reducing noise.

Ideally, the spatial resolution of an imager should be limited by the geometric pixel size. However, in most practical image detectors, resolutions are limited, not by geometric pixel sizes, but by cross-talk. (As used here, "cross-talk" denotes the response of a pixel to light focused on an adjacent pixel.) Cross-talk degrades spatial resolution of an imager, reduces overall sensitivity, compromises color fidelity, and leads to additional noise in the image after color correction. Diffusion cross-talk occurs where photogenerated charge carriers can move to neighboring charge-accumulation sites — in particular, where junction diodes in adjacent pixels have insufficient depletion widths.

The left side of the figure presents a schematic cross section of a typical conventional CMOS imager pixel containing a junction diode connected to the source of a reset MOSFET. The junction diode is formed between the n



The Proposed CMOS Imager Pixel device structure would be similar to the conventional one but would include deep p and n wells.

well and the p epitaxial layer (or p substrate). The n well is connected to the source of the reset MOSFET through an n⁺ implant. The reset MOSFET and an associate source-follower MOSFET are n-type and are placed inside a p well. For reasons too complex to present in this article, the depletion width is too small to prevent lateral diffusion of photo-induced charge carriers in the undepleted (field-free) epitaxial region. In the absence of a guiding electric field, photoelectrons generated in the epitaxial layer substrate diffuse omnidirectionally between pixels, thereby causing cross-talk.

The maximum supply potential in a CMOS process is between 3 and 5 V. When potential drops are taken into account, the reverse bias across the diode is between 2 and 3 V. At these reverse biases, the p-n junction depletion width is too small to prevent diffusion cross-

talk, especially for longer wavelength light. In principle, the depletion width could be increased significantly by applying a large reverse bias (e.g., 50 V) to the p epitaxial layer or substrate. However, because of (1) the electrical connection between the p well and the p epitaxial layer or substrate and (2) a requirement to keep at the most between 3 and 5 V across the CMOS devices, it is not possible to apply such a large reverse bias in this device structure. This prompts the proposed improvement in device structure.

A CMOS imager pixel as proposed, depicted on the right side of the figure, would include a deep n well and a deep p well in addition to the conventional n and p wells. The photodiode would be formed by the deep n well and the p epitaxial layer or substrate. The anode end (n end) of the diode would be connected to the n⁺ source

implant of the reset MOSFET through the conventional n well. The reset and source-follower MOSFETs would reside in the p well as in the conventional device structure.

Unlike in the conventional device structure, the deep n well would electrostatically separate the p well in the vertical direction from the p epitaxial layer or substrate. The horizontal isolation of photodiodes in adjacent pixels from each other would be achieved by the deep p wells: Each deep p well would establish a potential barrier that would prevent electrons in the deep n wells of adjacent pixels from communicating with each other.

Inasmuch as the conventional and deep p wells would both be electrosta-

tically isolated from the p epitaxial layer or substrate by the deep n well, any reverse (negative) bias could be applied to the p epitaxial layer or substrate without causing the potential difference between the n and p wells to increase beyond the typical conventional range of 2 to 3 V. Depending upon the resistivity of the substrate, a back-side reverse bias in excess of 50 V could be applied to achieve depletion widths as large as 50 μm , while the MOSFETs could be operated with conventional CMOS power supplies and biases. Thus, the incorporation of the deep n well and p well would allow the integration of a photodiode with a very large back-bias and very large depletion width alongside state-of-the-art

MOSFETs with small supply voltages, resulting in the development of high-performance CMOS imager sensors.

This work was done by Bedabrata Pain of Caltech for NASA's Jet Propulsion Laboratory.

In accordance with Public Law 96-517, the contractor has elected to retain title to this invention. Inquiries concerning rights for its commercial use should be addressed to:

*Innovative Technology Assets Management
JPL*

*Mail Stop 202-233
4800 Oak Grove Drive
Pasadena, CA 91109-8099
(818) 354-2240*

E-mail: iaoffice@jpl.nasa.gov

Refer to NPO-41226, volume and number of this NASA Tech Briefs issue, and the page number.

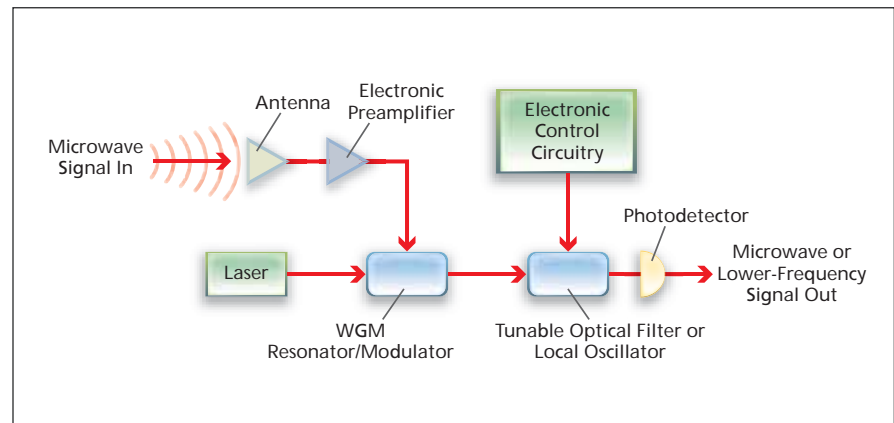
Wide-Band Microwave Receivers Using Photonic Processing

One receiver would have the functionality of multiple traditional heterodyne microwave receivers.

NASA's Jet Propulsion Laboratory, Pasadena, California

In wide-band microwave receivers of a type now undergoing development, the incoming microwave signals are electronically preamplified, then frequency-up-converted to optical signals that are processed photonically before being detected. This approach differs from the traditional approach, in which incoming microwave signals are processed by purely electronic means. As used here, "wide-band microwave receivers" refers especially to receivers capable of reception at any frequency throughout the range from about 90 to about 300 GHz. The advantage expected to be gained by following the up-conversion-and-photonic-processing approach is the ability to overcome the limitations of currently available detectors and tunable local oscillators in the frequency range of interest.

In a receiver following this approach (see figure), a preamplified incoming microwave signal is up-converted by the method described in the preceding article. The frequency up-converter exploits the nonlinearity of the electromagnetic response of a whispering-gallery-mode (WGM) resonator made of LiNbO_3 . Up-conversion takes place by three-wave mixing in the resonator. The WGM resonator is designed and fabricated to function simultaneously



A Microwave Signal Is Up-Converted to an optical signal, then filtered or otherwise processed photonically before being detected.

as an electro-optical modulator and to exhibit resonance at the microwave and optical operating frequencies plus phase matching among the microwave and optical signals circulating in the resonator. The up-conversion is an efficient process, and the efficiency is enhanced by the combination of microwave and optical resonances.

The up-converted signal is processed photonically by use of a tunable optical filter or local oscillator, and is then detected. Tunable optical filters can be made to be frequency agile and to exhibit high resonance quality factors (high Q values), thereby making it possi-

ble to utilize a variety of signal-processing modalities. Therefore, it is anticipated that when fully developed, receivers of this type will be compact and will be capable of both wide-band and narrow-band signal processing. Thus, one compact receiver of this type would afford the functionality that, heretofore, could have been obtained only by use of multiple heterodyne microwave receivers.

This work was done by Andrey Matsko, Lute Maleki, Vladimir Itchenko, Nan Yu, Dmitry Strekalov, and Anatoliy Savchenkov of Caltech for NASA's Jet Propulsion Laboratory. For more information, contact iaoffice@jpl.nasa.gov. NPO-45313



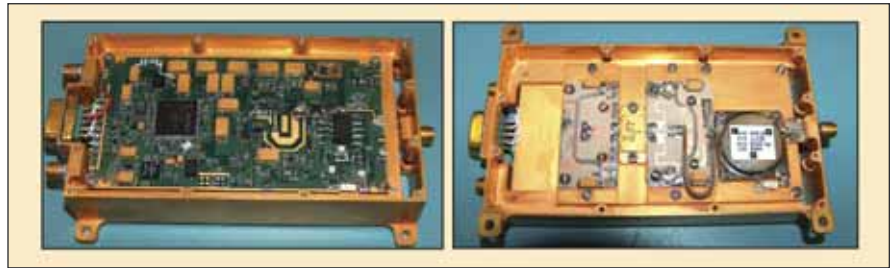
L-Band Transmit/Receive Module for Phase-Stable Array Antennas

A self-calibrating interferometric synthetic aperture radar instrument uses an electronically steerable radar antenna to achieve greater accuracy.

NASA's Jet Propulsion Laboratory, Pasadena, California

Interferometric synthetic aperture radar (InSAR) has been shown to provide very sensitive measurements of surface deformation and displacement on the order of 1 cm. Future systematic measurements of surface deformation will require this capability over very large areas (300 km) from space. To achieve these required accuracies, these spaceborne sensors must exhibit low temporal decorrelation and be temporally stable systems. An L-band (24-cm-wavelength) InSAR instrument using an electronically steerable radar antenna is suited to meet these needs. In order to achieve the 1-cm displacement accuracy, the phased array antenna requires phase-stable transmit/receive (T/R) modules. The T/R module operates at L-band (1.24 GHz) and has less than 1-deg absolute phase stability and less than 0.1-dB absolute amplitude stability over temperature. The T/R module is also high power (30 W) and power efficient (60-percent overall efficiency). The design is currently implemented using discrete components and surface mount technology.

The basic T/R module architecture is augmented with a calibration loop to



The photo shows the T/R Module on the front side and the 30-W Power Amp on the reverse side.

compensate for temperature variations, component variations, and path loss variations as a function of beam settings. The calibration circuit consists of an amplitude and phase detector, and other control circuitry, to compare the measured gain and phase to a reference signal and uses this signal to control a precision analog phase shifter and analog attenuator. An architecture was developed to allow for the module to be bidirectional, to operate in both transmit and receive mode. The architecture also includes a power detector used to maintain a transmitter power output constant within 0.1 dB.

The use of a simple, stable, low-cost, and high-accuracy gain and phase de-

tor made by Analog Devices (AD8302), combined with a very-high-efficiency T/R module, is novel. While a self-calibrating T/R module capability has been sought for years, a practical and cost-effective solution has never been demonstrated. By adding the calibration loop to an existing high-efficiency T/R module, there is a demonstrated order-of-magnitude improvement in the amplitude and phase stability.

This work was done by Constantine Andricos and Wendy Edelstein of Caltech and Vladimir Krimskiy of Santa Barbara Applied Research for NASA's Jet Propulsion Laboratory. Further information is contained in a TSP (see page 1).NPO-45147

Microwave Power Combiner/Switch Utilizing a Faraday Rotator

Either or both of two input ports could be coupled to one output port.

NASA's Jet Propulsion Laboratory, Pasadena, California

A proposed device for combining or switching electromagnetic beams would have three ports, would not contain any moving parts, and would be switchable among three operating states:

- Two of the ports would be for input; the remaining port would be for output.
- In one operating state, the signals at both input ports would be coupled through to the output port.
- In each of the other two operating states, the signal at only one input port

would be coupled to the output port. The input port would be selected through choice of the operating state.

In one potential application, the device would be used to switch or combine microwave signals in a quasi-optical transmission-line assembly that would be part of a millimeter-wave radar or telecommunication system. In another potential application, a modified version of the device would be used to switch or combine light signals in a fiber-optic telecommunication link.

The two input ports would be configured to accommodate signals having mutually orthogonal linear polarizations. A polarizer would be positioned to bisect the right angle formed by the longitudinal axes of the input ports, and its polarization would be oriented to so that it would allow one input signal to pass through and would reflect the other input signal. The orientations of the aforementioned components would be such that after impinging on the polarizer, both input signals would propagate

toward a three-state Faraday rotator. The components of the Faraday rotator would be a ferrite disk, a solenoidal electromagnet coil for applying magnetic bias, and two impedance-matching plates — one on each side of the ferrite disk. The output port would be positioned on the side opposite the input side of the Faraday rotator and would be oriented to support polarization at an angle of 45° relative to both of the input polarizations.

The operating state would be selected by adjusting the magnetic bias to select one of three states of the Faraday rotator. In one state, the magnetic bias would be set to cause the polarization of a propagating signal to rotate through an angle of +45° so as to allow one of the

input signals to propagate to the output port. In another state, the direction of the magnetic bias would be set at the reverse of that of the first-mentioned state to obtain a polarization rotation of 45°, thereby allowing the other input signal to propagate to the output port.

The third state would be used for combining the powers of two mutually coherent input signals that, in an ideal case, would be of equal magnitude and would differ in phase by 90°. In this state, the magnetic bias (and thus, the Faraday rotation) would be set to zero and the superposition of the input signals would result in a 45°-polarized sum signal that would propagate to the output port. In practice, because of magnetic hysteresis, this state could not be obtained by simply abruptly

turning off the current in the electromagnet: It would be necessary to apply a damped sinusoidal excitation to the electromagnet coil to effect degaussing.

This work was done by Raul Perez of Caltech for NASA's Jet Propulsion Laboratory.

In accordance with Public Law 96-517, the contractor has elected to retain title to this invention. Inquiries concerning rights for its commercial use should be addressed to:

*Innovative Technology Assets Management
JPL*

Mail Stop 202-233

4800 Oak Grove Drive

Pasadena, CA 91109-8099

E-mail: iaoffice@jpl.nasa.gov

Refer to NPO-44316, volume and number of this NASA Tech Briefs issue, and the page number.

Compact Low-Loss Planar Magic-T

These wireless communications components are useful for base-station receivers, consumer electronics, and industrial microwave instrumentation.

Goddard Space Flight Center, Greenbelt, Maryland

This design allows broadband power combining with high isolation between the H port and E port, and achieves a lower insertion loss than any other broadband planar magic-T. Passive microwave/millimeter-wave signal power is combined both in-phase and out-of-phase at the ports, with the phase error being less than ±1°, which is limited by port impedance.

The in-phase signal combiner consists of two quarter-wavelength-long transmission lines combined at the microstrip line junction. The out-of-phase signal combiner consists of two half-wavelength-long transmission lines combined in series. Structural symmetry creates a virtual

ground plane at the combining junction, and the combined signal is converted from microstrip line to slotline. Optimum realizable characteristic impedances are used so that the magic-T provides broadband response with low return loss.

The magic-T is used in microwave and millimeter-wave frequencies, with the operating bandwidth being approximately 100 percent. The minimum isolation obtainable is 32 dB from port E to port H. The magic-T VSWR is less than 1.1 in the operating band. Operating temperature is mainly dependent on the variation in the dielectric constant of the substrate. Using crystallized substrate, the invention can operate in an ex-

tremely broad range of temperatures (from 0 to 400 K). It has a very high reliability because it has no moving parts and requires no maintenance, though it is desirable that the magic-T operate in a low-humidity environment. Fabrication of this design is very simple, using only two metallized layers. No bond wires, via holes, or air bridges are required. Additionally, this magic-T can operate as an individual component without auxiliary components.

This work was done by Kongpop U-yen, Edward J. Wollack, Terence Doiron, and Samuel H. Moseley of Goddard Space Flight Center. Further information is contained in a TSP (see page 1). GSC-15353-1

Using Pipelined XNOR Logic to Reduce SEU Risks in State Machines

Risk is reduced by use of fast state-machine and error-detection logic.

NASA's Jet Propulsion Laboratory, Pasadena, California

Single-event upsets (SEUs) pose great threats to avionic systems' state machine control logic, which are frequently used to control sequence of events and to qualify protocols. The risks of SEUs manifest in two ways: (a) the state machine's state information is changed, causing the state

machine to unexpectedly transition to another state; (b) due to the asynchronous nature of SEU, the state machine's state registers become metastable, consequently causing any combinational logic associated with the metastable registers to malfunction temporarily. Effect (a) can

be mitigated with methods such as triple-modular redundancy (TMR). However, effect (b) cannot be eliminated and can degrade the effectiveness of any mitigation method of effect (a).

Although there is no way to completely eliminate the risk of SEU-in-

duced errors, the risk can be made very small by use of a combination of very fast state-machine logic and error-detection logic. Therefore, one goal of two main elements of the present method is to design the fastest state-machine logic circuitry by basing it on the fastest generic state-machine design, which is that of a one-hot state machine. The other of the two main design elements is to design fast error-detection logic circuitry and to optimize it for implementation in a

field-programmable gate array (FPGA) architecture: In the resulting design, the one-hot state machine is fitted with a multiple-input XNOR gate for detection of illegal states. The XNOR gate is implemented with lookup tables and with pipelines for high speed.

In this method, the task of designing all the logic must be performed manually because no currently available logic-synthesis software tool can produce optimal solutions of design problems of this

type. However, some assistance is provided by a script, written for this purpose in the Python language (an object-oriented interpretive computer language) to automatically generate hardware description language (HDL) code from state-transition rules.

This work was done by Martin Le, Xin Zheng, and Sunant Katanyoutant of Caltech for NASA's Jet Propulsion Laboratory. Further information is contained in a TSP (see page 1). NPO-42401

Quasi-Optical Transmission Line for 94-GHz Radar

This apparatus functions as a very-low-loss, three-port circulator.

NASA's Jet Propulsion Laboratory, Pasadena, California

A quasi-optical transmission line (QOTL) has been developed as a low-loss transmission line for a spaceborne cloud-observing radar instrument that operates at a nominal frequency of 94 GHz. This QOTL could also readily be redesigned for use in terrestrial millimeter-wave radar systems and millimeter-wave imaging systems.

In the absence of this or another low-loss transmission line, it would be necessary to use a waveguide transmission line in the original radar application. Unfortunately, transmission losses increase and power-handling capacities of waveguides generally decrease with frequency, such that at 94 GHz, the limitation on transmitting power and the combined transmission and reception losses (> 5 dB) in a waveguide transmis-

sion line previously considered for the original application would be unacceptable.

The QOTL functions as a very-low-loss, three-port circulator. The QOTL includes a shaped input mirror that can be rotated to accept 94-GHz transmitter power from either of two high-power amplifiers. Inside the QOTL, the transmitter power takes the form of a linearly polarized beam radiated from a feed horn. This beam propagates through a system of mirrors, each of which refocuses the beam to minimize diffraction losses. A magnetically biased ferrite disc is placed at one of the foci to utilize the Faraday effect to rotate the polarization of the beam by 45°. The beam is then transmitted via an antenna system.

The radar return (scatter from clouds, and/or reflections from other objects) is collected by the same antenna and propagates through the Faraday rotator in the reverse of the direction of propagation of the transmitted beam. In the Faraday rotator, the polarization of the received signal is rotated a further 45°, so that upon emerging from the Faraday rotator, the received beam is polarized at 90° with respect to the transmitted beam. The transmitted and received signals are then separated by a wire-grid polarizer.

This work was done by Raul M. Perez and Watt Veruttipong of Caltech for NASA's Jet Propulsion Laboratory. For more information, contact iaoffice@jpl.nasa.gov. NPO-44236

Next Generation Flight Controller Trainer System

Lyndon B. Johnson Space Center, Houston, Texas

The Next Generation Flight Controller Trainer (NGFCT) is a relatively inexpensive system of hardware and software that provides high-fidelity training for space-shuttle flight controllers. NGFCT provides simulations into which are integrated the behaviors of emulated space-shuttle vehicle onboard general-purpose computers (GPCs), mission-control center (MCC) displays, and space-shuttle systems as represented by high-fidelity shuttle mission

simulator (SMS) mathematical models. The emulated GPC computers enable the execution of onboard binary flight-specific software. The SMS models include representations of system malfunctions that can be easily invoked. The NGFCT software has a flexible design that enables independent updating of its GPC, SMS, and MCC components.

This work was done by Scott Arnold, Matthew R. Barry, Isaac Benton, Michael M.

Bishop, Steven Evans, Jason Harvey, Timothy King, Jacob Martin, Al Mercier, Walt Miller, Dan L. Payne, Hanh Phu, James C. Thompson, and Ron Aadsen of United Space Alliance for Johnson Space Center. Further information is contained in a TSP (see page 1). MSC-23617-1



➤ **Converting From DDOR SASF to APF**

A computer program called “ddor_sasf2apf” converts delta-door (delta differential one-way range) request from an SASF (spacecraft activity sequence file) format to an APF (apgen plan file) format for use in the Mars Reconnaissance Orbiter (MRO) mission-planning-and-sequencing process. The APF is used as an input to “APGEN/AUTOGEN” in the MRO activity-planning and command-sequence-generating process to sequence the delta-door (DDOR) activity. The DDOR activity is a spacecraft tracking technique for determining spacecraft location.

The input to ddor_sasf2apf is an input request SASF provided by an observation team that utilizes DDOR. ddor_sasf2apf parses this DDOR SASF input, rearranging parameters and reformatting the request to produce an APF file for use in AUTOGEN and/or APGEN. The benefit afforded by ddor_sasf2apf is to enable the use of the DDOR SASF file earlier in the planning stage of the command-sequence-generating process and to produce sequences, optimized for DDOR operations, that are more accurate and more robust than would otherwise be possible.

This program was written by Roy E. Gladden, Teerapat Khanampornpan, and Forest W. Fisher of Caltech for NASA's Jet Propulsion Laboratory.

This software is available for commercial licensing. Please contact Karina Edmonds of the California Institute of Technology at (626) 395-2322. Refer to NPO-45413.

➤ **Converting From CVF to AAF**

A computer program called “dsn config converter” automates what had been a manual process for updating the multi-mission adaptation file (multi.aaf) used by a multiple-mission-command-sequence-generating process comprised of a combination of the AUTOGEN and APGEN programs mentioned in the immediately preceding article. The program converts the dsn_config.cvf file that provides DSN (Deep Space Network) antenna configuration code mappings from a context variable file (CVF) format used in another part of the command genera-

tion process to an APGEN activity file (AAF) format used by AUTOGEN and APGEN.

Whereas previously, the information in the dsn_config.cvf file was manually encoded into the multi.aaf file, now the program automatically generates a dsn_config.aaf file from the dsn_config.cvf file. As part of this development effort the multi.aaf file was adapted to use the new dsn_config.aaf representations. Through this automation a tedious error-prone step has now been replaced by a quick and robust step.

This program was written by Roy E. Gladden, Teerapat Khanampornpan, and Forest W. Fisher of Caltech for NASA's Jet Propulsion Laboratory.

This software is available for commercial licensing. Please contact Karina Edmonds of the California Institute of Technology at (626) 395-2322. Refer to NPO-45423.

➤ **Documenting AUTOGEN and APGEN Model Files**

A computer program called “autogen hypertext map generator” satisfies a need for documenting and assisting in visualization of, and navigation through, model files used in the AUTOGEN and APGEN software mentioned in the two immediately preceding articles. This program parses autogen script files, autogen model files, PERL scripts, and apgen activity-definition files and produces a hypertext map of the files to aid in the navigation of the model. This program also provides a facility for adding notes and descriptions, beyond what is in the source model represented by the hypertext map. Further, this program provides access to a summary of the model through variable, function, sub routine, activity and resource declarations as well as providing full access to the source model and source code. The use of the tool enables easy access to the declarations and the ability to traverse routines and calls while analyzing the model.

This program was written by Roy E. Gladden, Teerapat Khanampornpan, Forest W. Fisher, and Chris C. Del Guercio of Caltech for NASA's Jet Propulsion Laboratory.

This software is available for commercial licensing. Please contact Karina Edmonds of the California Institute of Technology at (626) 395-2322. Refer to NPO-45424.

➤ **Sequence History Update Tool**

The Sequence History Update Tool performs Web-based sequence statistics archiving for Mars Reconnaissance Orbiter (MRO). Using a single UNIX command, the software takes advantage of sequencing conventions to automatically extract the needed statistics from multiple files. This information is then used to populate a PHP database, which is then seamlessly formatted into a dynamic Web page.

This tool replaces a previous tedious and error-prone process of manually editing HTML code to construct a Web-based table. Because the tool manages all of the statistics gathering and file delivery to and from multiple data sources spread across multiple servers, there is also a considerable time and effort savings. With the use of The Sequence History Update Tool what previously took minutes is now done in less than 30 seconds, and now provides a more accurate archival record of the sequence commanding for MRO.

This work was done by Teerapat Khanampornpan, Roy Gladden, Forest Fisher, and Chris Del Guercio of Caltech for NASA's Jet Propulsion Laboratory.

This software is available for commercial licensing. Please contact Karina Edmonds of the California Institute of Technology at (626) 395-2322. Refer to NPO-45288.

➤ **Extraction and Analysis of Display Data**

The Display Audit Suite is an integrated package of software tools that partly automates the detection of Portable Computer System (PCS) Display errors. [PCS is a laptop computer used onboard the International Space Station (ISS).] The need for automation stems from the large quantity of PCS displays (6,000+, with 1,000,000+ lines of command and telemetry data). The Display Audit Suite includes data-extraction tools, automatic error detection tools, and database tools for generating analysis spreadsheets.

These spreadsheets allow engineers to more easily identify many different kinds of possible errors. The Suite supports over 40 independent analyses,

and complements formal testing by being comprehensive (all displays can be checked) and by revealing errors that are difficult to detect via test. In addition, the Suite can be run early in the development cycle to find and correct errors in advance of testing.

This software suite was developed by Chris Land of The Boeing Company and Kathryn Moyer of the Dynacs Co. for Johnson Space Center. Further information is contained in a TSP (see page 1). MSC-23630-1

➤ MRO DKF Post-Processing Tool

This software tool saves time and reduces risk by automating two labor-intensive and error-prone post-processing steps required for every DKF [DSN (Deep Space Network) Keyword File] that MRO (Mars Reconnaissance Orbiter) produces, and is being extended to post-process the corresponding TSOE (Text Sequence Of Events) as well. The need for this post-processing step stems from limitations in the seqgen modeling resulting in incorrect DKF generation that is then cleaned up in post-processing.

This work was done by Shanti Ayap of LMCO, and Forest Fisher, Roy Gladden, and Teerapat Khanampornpan of NASA's Jet Propulsion Laboratory.

This software is available for commercial licensing. Please contact Karina Edmonds of the California Institute of Technology at (626) 395-2322. Refer to NPO-45481.

➤ Rig Diagnostic Tools

Rig Diagnostic Tools is a suite of applications designed to allow an operator to monitor the status and health of complex networked systems using a unique interface between Java applications and UNIX scripts. The suite consists of Java applications, C scripts, VxWorks applications, UNIX utilities, C programs, and configuration files. The UNIX scripts retrieve data from the system and write them to a certain set of files. The Java side monitors these files and presents the data in user-friendly formats for operators to use in making troubleshooting decisions. This design allows for rapid prototyping and expansion of higher-level displays without affecting the basic data-gathering applications. The suite is designed to be extensible, with the ability to add new system components

in building block fashion without affecting existing system applications. This allows for monitoring of complex systems for which unplanned shutdown time comes at a prohibitive cost.

This program was written by Kerry M. Soileau of Johnson Space Center and John W. Baicy of The Boeing Co. Further information is contained in a TSP (see page 1). MSC-24158-1

➤ MRO Sequence Checking Tool

The MRO Sequence Checking Tool program, `mro_check`, automates significant portions of the MRO (Mars Reconnaissance Orbiter) sequence checking procedure. Though MRO has similar checks to the ODY's (Mars Odyssey) Mega Check tool, the checks needed for MRO are unique to the MRO spacecraft.

The MRO sequence checking tool automates the majority of the sequence validation procedure and check lists that are used to validate the sequences generated by MRO MPST (mission planning and sequencing team). The tool performs more than 50 different checks on the sequence. The automation varies from summarizing data about the sequence needed for visual verification of the sequence, to performing automated checks on the sequence and providing a report for each step. To allow for the addition of new checks as needed, this tool is built in a modular fashion.

This work was done by Forest Fisher, Roy Gladden, and Teerapat Khanampornpan of Caltech for NASA's Jet Propulsion Laboratory.

This software is available for commercial licensing. Please contact Karina Edmonds of the California Institute of Technology at (626) 395-2322. Refer to NPO-45480.

➤ Science Activity Planner for the MER Mission

The Maestro Science Activity Planner is a computer program that assists human users in planning operations of the Mars Explorer Rover (MER) mission and visualizing scientific data returned from the MER rovers. Relative to its predecessors, this program is more powerful and easier to use. This program is built on the Java Eclipse open-source platform around a Web-browser-based user-interface paradigm to provide an intuitive user interface to Mars rovers and landers.

This program affords a combination of advanced display and simulation capabilities. For example, a map view of terrain can be generated from images acquired by the High Resolution Imaging Science Explorer instrument aboard the Mars Reconnaissance Orbiter spacecraft and overlaid with images from a navigation camera (more precisely, a stereoscopic pair of cameras) aboard a rover, and an interactive, annotated rover traverse path can be incorporated into the overlay. It is also possible to construct an overhead perspective mosaic image of terrain from navigation-camera images.

This program can be adapted to similar use on other outer-space missions and is potentially adaptable to numerous terrestrial applications involving analysis of data, operations of robots, and planning of such operations for acquisition of scientific data.

This program was written by Jeffrey S. Norris, Thomas M. Crockett, Jason M. Fox, Joseph C. Joswig, Mark W. Powell, Khawaja S. Shams, Recaredo J. Torres, Michael N. Wallick, and David S. Mittman of Caltech for NASA's Jet Propulsion Laboratory.

This software is available for commercial licensing. Please contact Karina Edmonds of the California Institute of Technology at (626) 395-2322. Refer to NPO-45871.

➤ UAVSAR Flight-Planning System

A system of software partly automates planning of a flight of the Uninhabited Aerial Vehicle Synthetic Aperture Radar (UAVSAR) — a polarimetric synthetic-aperture radar system aboard an unpiloted or minimally piloted airplane. The software constructs a flight plan that specifies not only the intended flight path but also the setup of the radar system at each point along the path.

A user first specifies the desired image swath by specifying certain geographic and geometric features of the swath or the desired flight path. Using an input digital elevation map (DEM), the software predicts the image swath and sets such variables as a data window position (DWP). A raster backscatter classification file co-registered with the input DEM can be used to estimate radar attenuation settings. The software determines whether such radar constraints as those pertaining to duty cycles and data rates are obeyed, and de-

termines when radar settings should be modified (for example, a DWP changed, or gain changed in response to a change in expected backscatter). The software constructs a Web page to facilitate transfer of radar control files

and to provide access to Keyhole Markup Language files, which can be used to display the flight path and associated information.

This program was written by Joanne G. Shimada, Anhua J. Chu, Elaine Chapin,

Scott Hensley, and Bruce D. Chapman of Caltech for NASA's Jet Propulsion Laboratory.

This software is available for commercial licensing. Please contact Karina Edmonds of the California Institute of Technology at (626) 395-2322. Refer to NPO-45877.



Templates for Deposition of Microscopic Pointed Structures

These structures can be used as field emitters in plasma television screens.

Goddard Space Flight Center, Greenbelt, Maryland

Templates for fabricating sharply pointed microscopic peaks arranged in nearly regular planar arrays can be fabricated by a relatively inexpensive technique that has recently been demonstrated. Depending on the intended application, a semiconducting, insulating, or metallic film could be deposited on such a template by sputtering, thermal evaporation, pulsed laser deposition, or any other suitable conventional deposition technique. Pointed structures fabricated by use of these techniques may prove useful as photocathodes or field emitters in plasma television screens. Selected peaks could be removed from such structures and used individually as scanning tips in atomic force microscopy or mechanical surface profiling.

The equipment and materials needed to form a template include the following:

- Several small plates (e.g., microscope slides) made of a suitable (preferably transparent) rigid material such as glass, quartz, or sapphire;
- Two permanent magnets that produce a flux density of the order of 1

kG (0.1 T) with an acceptably low spatial variation over an area at least as large as that of the template to be formed; and

- A ferrofluid (consisting of Fe_2O_3 particles suspended in an oil-based solution that includes a surfactant).

A small quantity (≈ 1 mL) of the ferrofluid is either dropped or spun onto one of the plates. The plate is oriented horizontally, supported by two other plates, positioned so that the ferrofluid-covered spot sits directly over one of the magnets. Next, using a combination of three other plates, the other magnet is positioned a short distance above the ferrofluid-covered spot (see Figure 1). The surface of the ferrofluid becomes deformed into an array of peaks generally oriented along magnetic-field lines. The positions of the magnets relative to each other and to the ferrofluid are adjusted to minimize nonuniformity in the array of peaks and to maximize the aspect ratio of the peaks. Next, the ferrofluid is dried in room air using a gently blowing muffin fan. The ferrofluid is then further dried and hardened in a thermal evaporation chamber pumped

down to a pressure of about 10^{-6} torr (about 1.3×10^{-4} Pa).

The resulting structure is ready for use as a template for deposition. For example, Figure 2 shows selected views of such a template that has been coated with thermally evaporated silver.

This work was done by Diane E. Pugel of Goddard Space Flight Center. Further information is contained in a TSP (see page 1).

This invention is owned by NASA, and a patent application has been filed. Inquiries concerning nonexclusive or exclusive license for its commercial development should be addressed to the Patent Counsel, Goddard Space Flight Center, (301) 286-7351. Refer to GSC-14871-1.

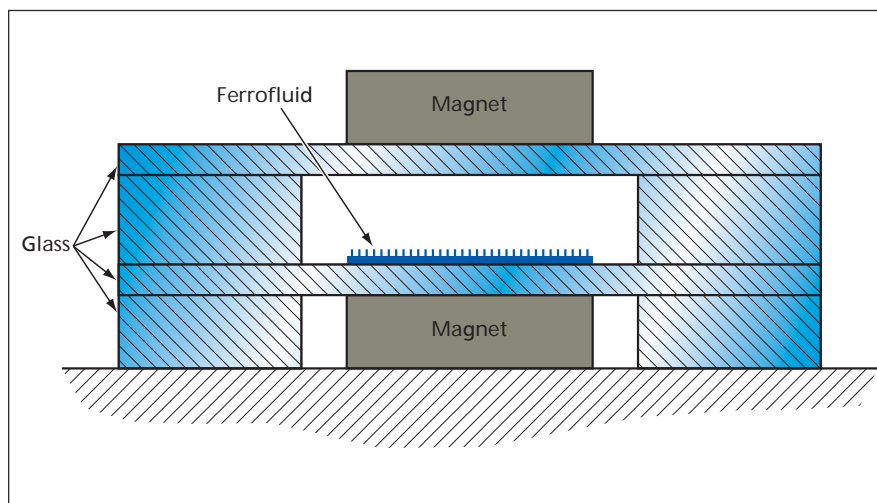


Figure 1. A Spot of Ferrofluid on a Plate is positioned between two magnets. The magnetic field deforms the upper surface of the ferrofluid into an array of peaks.

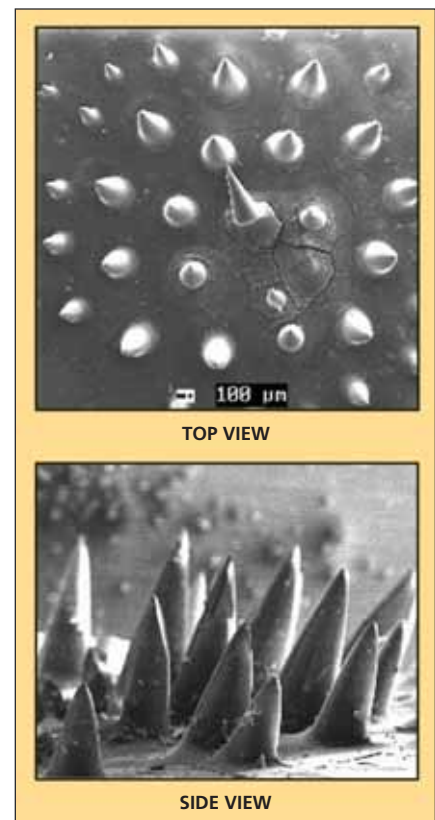


Figure 2. A Portion of a Template fabricated as described in the text is shown here in top-view and side-view scanning electron micrographs.



Adjustable Membrane Mirrors Incorporating G-Elastomers

NASA's Jet Propulsion Laboratory, Pasadena, California

Lightweight, flexible, large-aperture mirrors of a type being developed for use in outer space have unimorph structures that enable precise adjustment of their surface figures. A mirror of this type includes a reflective membrane layer bonded with an electrostrictive grafted elastomer (G-elastomer) layer, plus electrodes suitably positioned with respect to these layers. By virtue of the electrostrictive effect, an electric field applied to the G-elastomer membrane induces a strain along the membrane and thus causes a deflection

of the mirror surface. Utilizing this effect, the mirror surface figure can be adjusted locally by individually addressing pairs of electrodes.

G-elastomers, which were developed at NASA Langley Research Center, were chosen for this development in preference to other electroactive polymers partly because they offer superior electro-mechanical performance. Whereas other electroactive polymers offer, variously, large strains with low moduli of elasticity or small strains with high moduli of elasticity, G-elastomers offer both large strains

(as large as 4 percent) and high moduli of elasticity (about 580 MPa). In addition, G-elastomer layers can be made by standard melt pressing or room-temperature solution casting.

This work was done by Zensheu Chang and Rhonda M. Morgan of Caltech, Eui-Hyeok Yang of Stevens Institute of Technology, Yoshikazu Hishinuma of Fuji Film Corp., and Ji Su and Tian-Bing Xu of NASA Langley Research Center for NASA's Jet Propulsion Laboratory. For more information, contact iaoffice@jpl.nasa.gov. NPO-45616

Hall-Effect Thruster Utilizing Bismuth as Propellant

Marshall Space Flight Center, Alabama

A laboratory-model Hall-effect spacecraft thruster was developed that utilizes bismuth as the propellant. Xenon was used in most prior Hall-effect thrusters. Bismuth is an attractive alternative because it has a larger atomic mass, a larger electron-impact-ionization cross-section, and is cheaper and more plentiful.

The design of this thruster includes multiple temperature-control zones and other features that reduce parasitic power losses. Liquid bismuth (which

melts at a temperature of 271°C) is supplied by a temperature-controlled reservoir to a vaporizer. The vaporizer exhausts to an anode/gas distributor inside a discharge channel that consists of a metal chamber upstream of ceramic exit rings. In the channel, bismuth ions are produced through an electron impact ionization process and accelerated as in other Hall-effect thrusters. The discharge region is heated by the discharge and an auxiliary anode heater, which is required to prevent bismuth condensa-

tion at low power levels and at thruster start-up. A xenon discharge is also used for preheating the discharge channel, but an anode heater could provide enough power to start the bismuth discharge directly.

This work was done by James Szabo, Charles Gasdaska, Vlad Hruby, and Mike Robin of Busek Co., Inc. for Marshall Space Flight Center. For further information, contact Sammy Nabors, MSFC Commercialization Assistance Lead, at sammy.a.nabors@nasa.gov. Refer to MFS-32440-1.

High-Temperature Crystal-Growth Cartridge Tubes Made by VPS

Mechanical properties and maximum useful temperature exceed those of tungsten-alloy tubes.

Marshall Space Flight Center, Alabama

Cartridge tubes for use in a crystal-growth furnace at temperatures as high as 1,600°C have been fabricated by vacuum plasma spraying (VPS). These cartridges consist mainly of an alloy of 60 weight percent molybdenum with 40 weight percent rhenium, made from molybdenum powder coated with rhenium. This alloy was selected because of its high melting temperature

(≈2,550°C) and because of its excellent ductility at room temperature. These cartridges are intended to supplant tungsten/nickel-alloy cartridges, which cannot be used at temperatures above ≈1,300°C.

Graphite mandrels were used as substrates for VPS to form the cartridge tubes to the desired size and shape. A mandrel was placed in the

VPS chamber, oriented vertically. Before spraying, the plasma gun was used to heat the mandrel to a temperature of about 1,093°C. Then, the Mo/Re alloy precursor powder was deposited by VPS on the mandrel to a thickness between 0.51 and 0.64 mm. The deposition was done in one pass, spraying from the top to the bottom of the mandrel.

Then a tantalum coat was deposited in a similar manner onto the Mo/Re deposit to a thickness between 0.13 and 0.18 mm. The tantalum coat serves as a sealing layer, increasing the protection of the Mo/Re alloy against the formation of such volatile oxides as MoO₃.

Next, the pressure in the chamber was reduced to <100 mtorr (less than about 13 Pa) and the cartridge allowed to cool. Once the cartridge had cooled to room temperature, the chamber was

opened to the atmosphere and the cartridge was removed from the mandrel.

A cross section of a representative cartridge tube fabricated in this process showed a good bond between the tantalum coat and the main body of Mo/Re alloy. Both the Mo/Re and the Ta were dense. Because this tube was not heat treated, the Mo/Re-alloy layer still contained two phases — one Mo-rich and one Re-rich. Tests of the mechanical properties of tubes like this

one in the as-sprayed condition have revealed a vast improvement over similar tungsten-alloy tubes in the as-sprayed condition.

This work was done by Richard Holmes of Marshall Space Flight Center and Scott O'Dell, Timothy McKechnie, and Christopher Power of Plasma Processes, Inc. For further information, contact Sammy Nabors, MSFC Commercialization Assistance Lead, at sammy.a.nabors@nasa.gov. MFS-31540-1

Quench Crucibles Reinforced With Metal

Specimens can be quenched rapidly, without cracking ampules.

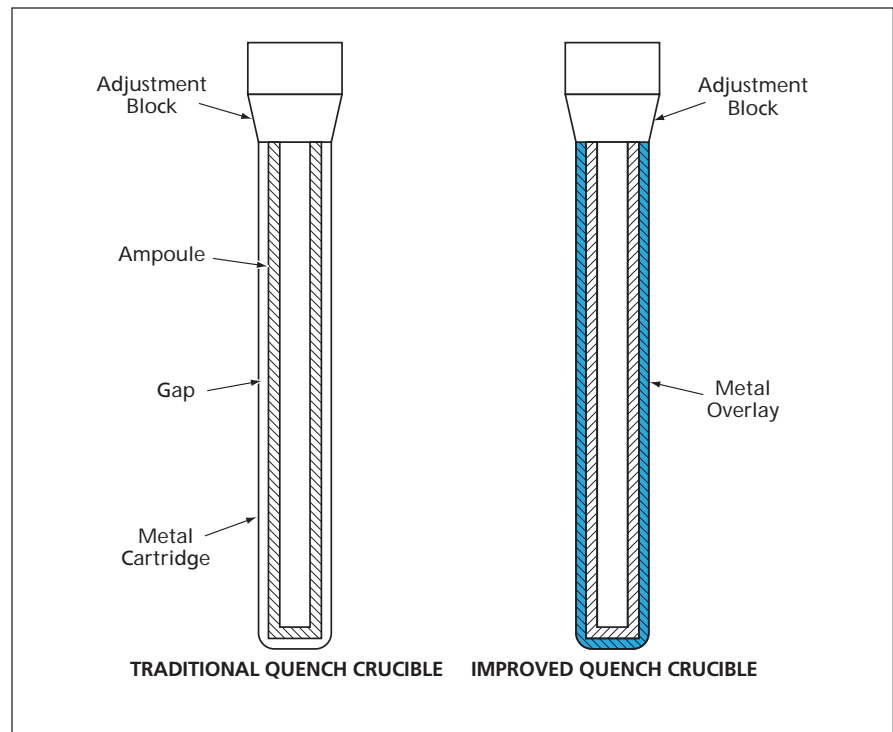
Marshall Space Flight Center, Alabama

Improved crucibles consisting mainly of metal-reinforced ceramic ampules have been developed for use in experiments in which material specimens are heated in the crucibles to various high temperatures, then quenched by, for example, plunging the crucibles into water at room temperature. A quench crucible of the traditional type intended to be supplanted by the improved crucibles consists mainly of a ceramic or graphite ampule inside a metal cartridge, with a gap between the metal and the cartridge, as shown on the left side of the figure.

The need for the improved quench crucibles arises as follows: In a traditional quench crucible, the gap between the ampule and the metal cartridge impedes the transfer of heat to such a degree that the quench rate (the rate of cooling of the specimen) can be too low to produce the desired effect in the specimen. One can increase the quench rate by eliminating the metal cartridge to enable direct quenching of the ampule, but then the thermal shock of direct quenching causes cracking of the ampule.

In a quench crucible of the present improved type, there is no gap and no metal cartridge in the traditional sense. Instead, there is an overlay of metal in direct contact with the ampule, as shown on the right side of the figure. Because there is no gap between the metal overlay and the ampule, the heat-transfer rate can be much greater than it is in a traditional quench crucible. The metal overlay also reinforces the ampule against cracking.

The choice of ampule material and metal depends on the specific applica-



The Metal Cartridge and Gap surrounding the ampule are replaced with an overlay of metal in intimate contact with the ampule.

tion. In general, the ampule material should be chemically compatible with the specimen material. The overlay metal should be chosen to have a coefficient of thermal expansion (CTE) as close as possible to that of the ampule material. Examples of suitable ampule/metal-overlay material pairs include the following:

- graphite (CTE = $8.0 \times 10^{-6} \text{ K}^{-1}$) and stainless steel (CTE = $9.9 \times 10^{-6} \text{ K}^{-1}$)
- aluminum nitride (CTE = $5.2 \times 10^{-6} \text{ K}^{-1}$) and tungsten heavy alloy (CTE = $5.0 \times 10^{-6} \text{ K}^{-1}$) and
- silicon carbide (CTE = $4.5 \times 10^{-6} \text{ K}^{-1}$)

and tungsten heavy alloy (CTE = $5.0 \times 10^{-6} \text{ K}^{-1}$).

Several thermal-spray processes for applying metal overlays to ampules were investigated. Of these processes, vacuum plasma spraying was found to yield the best results.

This work was done by Richard R. Holmes and Edgar Carrasquillo of Marshall Space Flight Center and J. Scott O'Dell and Timothy N. McKechnie of Plasma Processes Inc. For further information, contact Sammy Nabors, MSFC Commercialization Lead, at sammy.a.nabors@nasa.gov. MFS-31598-1



Deep-Sea Hydrothermal-Vent Sampler

This apparatus collects hydrothermal-plume samples uncontaminated by surrounding water.

NASA's Jet Propulsion Laboratory, Pasadena, California

An apparatus is being developed for sampling water for signs of microbial life in an ocean hydrothermal vent at a depth of as much as 6.5 km. Heretofore, evidence of microbial life in deep-sea hydrothermal vents has been elusive and difficult to validate. Because of the extreme conditions in these environments (high pressures and temperatures often in excess of 300°C), deep-sea hydrothermal-vent samplers must be robust. Because of the presumed low density of biomass of these environments, samplers must be capable of collecting water samples of significant volume. It is also essential to prevent contamination of samples by microbes entrained from surrounding waters. Prior to the development of the present apparatus, no sampling device was capable of satisfying these requirements.

The apparatus (see figure) includes an intake equipped with a temperature probe, plus several other temperature probes located away from the intake. The readings from the temperature probes are utilized in conjunction with readings from flowmeters to determine the position of the intake relative to the hydrothermal plume and, thereby, to position the intake to sample directly from the plume. Because it is necessary to collect large samples of water in order to obtain sufficient microbial biomass but it is not practical to retain all the water from the samples, four filter arrays are used to concentrate the microbial biomass (which is assumed to consist of particles larger than 0.2 μm) into smaller volumes. The appa-

ratus can collect multiple samples per dive and is designed to process a total volume of 10 L of vent fluid, of which most passes through the filters, leaving a total possibly-microbe-containing sample volume of 200 mL remaining in filters.

A rigid titanium nose at the intake is used for cooling the sample water before it enters a flexible inlet hose connected to a pump. As the water passes through the titanium nose, it must be cooled to a temperature that is above a mineral-precipitation temperature of 100°C but below the upper working temperature (230°C) of switching valves and tubes in the apparatus. The sample water then passes into a manifold tube, from whence the switching valves can direct the water through either a bypass tube or any one of the filter arrays, without contamination from a previous sample. Each filter array consists of series of filters having pore sizes decreasing in the direction of flow: 90-, 60-, 15-, and 7- μm prefilters and a large-surface-area 0.2- μm collection filter. All the filter taps are located between the intake and the bypass tube so that each time the bypass tube is used, the entire manifold tube is flushed as well.

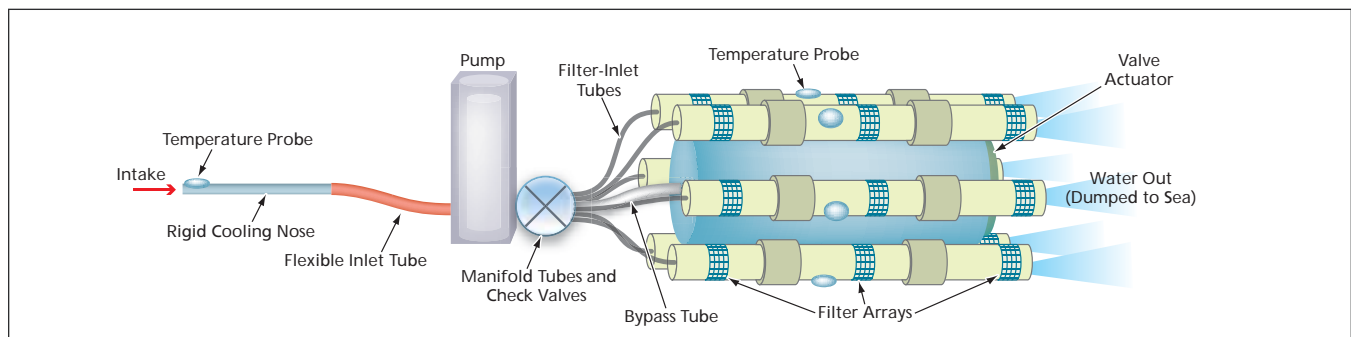
The switching valves include five passive ones (a check valve for the bypass tube for each of four filter arrays) at the upstream (manifold) end and an active one (a five-position actuated valve) at the downstream end. The incorporation of the check valves at the upstream end makes it unnecessary to use actuated valves at both ends. Once the actuated valve has been turned to the bypass position, the pump

begins to flush the intake and manifold of any particulate matter that may have accumulated. After flushing, sampling is started by setting the actuated valve to pass water through one of the filter arrays. The process of flushing and sampling is repeated for each of the four filter arrays.

Because the apparatus is rated to a depth of 6.5 km, it is pressure-compensated; as the pressure increases between atmospheric at the ocean surface and about 10 kpsi (≈ 69 MPa) at maximum depth, the volume of water within the system decreases by about 2.7 percent. A flexible membrane within the apparatus accommodates the compression and expansion of water upon descent and ascent, respectively.

The apparatus includes a system for monitoring and regulating temperatures, pressures, and flow rates throughout the system. This control and monitoring system includes a small microprocessor, motor controllers (for the pump and the valve actuator), the aforementioned temperature probes, pressure sensors, and a serial data link to a laptop computer aboard a submarine or other vessel used to bring the apparatus to and from the hydrothermal vent.

This work was done by Alberto E. Behar, Kasthur Venkateswaran, and Jaret B. Matthews of Caltech and Cesar Rivadeneyra, James C. Bruckner, Edmond So, and Goran Basic of the International Space University for NASA's Jet Propulsion Laboratory. Further information is contained in a TSP (see page 1).
NPO-42617



The Intake Is Positioned in the plume of a hydrothermal vent with the help of temperature-probe readings, then water is pumped from the intake through filter arrays to collect microbes.

⚙️ Mars Rocket Propulsion System

Marshall Space Flight Center, Alabama

A report discusses the methane and carbon monoxide/LOX (McLOx) rocket for ascent from Mars as well as other critical space propulsion tasks. The system offers a specific impulse over 370 s — roughly 50 s higher than existing space-storable bio-propellants. Current Mars *in-situ* propellant production (ISPP) technologies produce impure methane and carbon monoxide in various combinations. While separation and purification of methane fuel is possible, it adds complexity to the propellant production process and discards an otherwise useful fuel product. The McLOx makes such complex and wasteful

processes unnecessary by burning the methane/CO mixtures produced by the Mars ISPP systems without the need for further refinement.

Despite the decrease in rocket-specific impulse caused by the CO admixture, the improvement offered by concomitant increased propellant density can provide a net improvement in stage performance. One advantage is the increase of the total amount of propellant produced, but with a decrease in mass and complexity of the required ISPP plant. Methane/CO fuel mixtures also may be produced by reprocessing the organic wastes of a Moon base or a

space station, making McLOx engines key for a human Lunar initiative or the International Space Station (ISS) program. Because McLOx propellant components store at a common temperature, very lightweight and compact common bulkhead tanks can be employed, improving overall stage performance further.

This work was done by Robert Zubrin and Dan Harber of Pioneer Astronautics for Marshall Space Flight Center. For further information, contact Sammy Nabors, MSFC Commercialization Lead, at sammy.a.nabors@nasa.gov. MFS-32541-1

⚙️ Two-Stage Passive Vibration Isolator

NASA's Jet Propulsion Laboratory, Pasadena, California

The design and testing of a structural system were implemented to hold the optics of the planned Space Interferometry Mission (SIM) at positions and orientations characterized by vibrational translation and rotation errors of no more than a few nanometers or a few milliarcsseconds, respectively. Much of the effort was devoted to a test bed for verifying the predicted behavior of a vibration-isolation structural subsystem working together with an active control system for positioning and orienting the SIM optics.

There was considerable emphasis on the vibration-isolation subsystem, which was passive and comprised two stages. The main sources of vibration were six reaction wheels in an assembly denoted the "backpack." The first vibration-isolation stage consisted of hexapod isolator mounts — one for each reaction wheel — characterized by a natural vibration frequency of 10 Hz. The second stage was a set of three beams, disposed between the backpack and the structure that held the SIM optics, that were flexured such that they

transmitted only bending loads, with a natural vibrational frequency and damping of about 5 Hz and 4 percent, respectively. Preliminary test results were presented and characterized as demonstrating the effectiveness of the two-stage vibration-isolation design.

This work was done by Renaud Goullioud, Yekta Gursel, Timothy Neville, Allen J. Bronowicki, David Platus, and Rhonda MacDonald of Caltech for NASA's Jet Propulsion Laboratory. For more information, contact iaoffice@jpl.nasa.gov. NPO-30734

⚙️ Improved Thermal Design of a Compression Mold

John H. Glenn Research Center, Cleveland, Ohio

A compression tool used to make 1-in. (2.5-cm) diameter disks of high-temperature polymers was designed to be shorter and of larger diameter than conventional tools to reduce heat loss to the surrounding air, thus making more efficient use of applied heat. This system is less sensitive to the amount and quality of insulation than previous tools, provides more repeatable processing, and improves the quality of the samples produced. These improvements come without increasing the weight of the punch portion of the tool over that of a conventional version, an important quality when handling lower-viscosity resins.

In use, the base and body of the tool are assembled, and the polymer to be processed is placed into the body of the tool. The punch is inserted, and the assembled tool is placed into the press. A temperature/pressure profile appropriate to the nature of the polymer is applied. A series of computational and experimental runs were made using a conventional tool to validate the computational model. The new tool design was then modeled, and when the performance showed a marked improvement, the new tool was manufactured. A new series of experimental

runs showed that the thermal performance of the new tool agreed well with model predictions.

This work was done by Maria A. Kuczumski and James C. Johnston of Glenn Research Center and DeNise Hardy-Green of the University of Akron. Further information is contained in a TSP (see page 1).

Inquiries concerning rights for the commercial use of this invention should be addressed to NASA Glenn Research Center, Innovative Partnerships Office, Attn: Steve Fedor, Mail Stop 4-8, 21000 Brookpark Road, Cleveland, Ohio 44135. Refer to LEW-17990-1.

⚙️ Enhanced Pseudo-Waypoint Guidance for Spacecraft Maneuvers

NASA's Jet Propulsion Laboratory, Pasadena, California

An enhanced version of the scheme reported in "Pseudo-Waypoint Guidance for Proximity Spacecraft Maneuvers" (NPO-42753), *NASA Tech Briefs*, Vol. 31, No. 6 (June 2007), page 73 was developed. To recapitulate: the scheme provides algorithms for guidance and control (G&C) of a spacecraft maneuvering near a small astronomical body. The open-loop guidance problem is solved in advance or in real time by use of the pseudo-waypoint generation (PWG) method. Feedback control is implemented to track PWG tra-

jectories, in a manner that enables updating of G&C in a model-predictive manner. The scheme includes silent periods following each thruster firing.

The original version of the scheme provides for a fire-first, followed-by-silence sequence, which is disadvantageous in that the silence after final firing precludes reduction of any remaining velocity error — an unacceptable result in the case of a maneuver for which a specific final velocity is required. In the enhanced version, the scheme is augmented with a fire-second

technique, so that the final velocity can be established with a much higher precision because both the guidance and feedback firing can be performed and ceased at the final maneuver time.

This work was done by John Carson and Behçet Açıkmese of Caltech for NASA's Jet Propulsion Laboratory.

The software used in this innovation is available for commercial licensing. Please contact Karina Edmonds of the California Institute of Technology at (626) 395-2322. Refer to NPO-44276.



Altimetry Using GPS-Reflection/Occultation Interferometry

NASA's Jet Propulsion Laboratory, Pasadena, California

A Global Positioning System (GPS)-reflection/occultation interferometry was examined as a means of altimetry of water and ice surfaces in polar regions. In GPS-reflection/occultation interferometry, a GPS receiver aboard a satellite in a low orbit around the Earth is used to determine the temporally varying carrier-phase delay between (1) one component of a signal from a GPS transmitter propagating directly through the atmosphere just as the GPS transmitter falls below the horizon and (2) another

component of the same signal, propagating along a slightly different path, reflected at glancing incidence upon the water or ice surface.

The integer-cycle phase-difference ambiguity is resolved by noting that both signal components eventually collapse into a single component, representing zero phase difference. From the phase difference and the known positions of the two spacecraft as functions of time, an atmospheric correction obtained as the main data product

of the GPS-receiver mission, and basic geometry, the difference in length between the direct and reflection signal paths and the altitude of the effective specular-reflection point can be calculated. This method yields altitude at about 0.7-m precision with horizontal resolution of a few kilometers.

This work was done by Estel Cardellach, Manuel De La Torre, George A. Hajj, and Chi Ao of Caltech for NASA's Jet Propulsion Laboratory. For more information, contact iaoffice@jpl.nasa.gov. NPO-41551

Thermally Driven Josephson Effect

NASA's Jet Propulsion Laboratory, Pasadena, California

A concept is proposed of the thermally driven Josephson effect in superfluid helium. Heretofore, the Josephson effect in a superfluid has been recognized as an oscillatory flow that arises in response to a steady pressure difference between two superfluid reservoirs separated by an array of submicron-sized orifices, which act in unison as a single Josephson junction. Analogously, the thermally driven Josephson effect is an oscillatory flow that arises in response to a steady temperature difference.

The thermally driven Josephson effect is partly a consequence of a quantum-mechanical effect known as the fountain effect, in which a temperature difference in a superfluid is accompanied by a pressure difference. The thermally driven Josephson effect may have significance for the development of a high-resolution gyroscope based on the Josephson effect in a superfluid: If the pressure-driven Josephson effect were used, then the fluid on the high-pressure side would become

depleted, necessitating periodic interruption of operation to reverse the pressure difference. If the thermally driven Josephson effect were used, there would be no net flow and so the oscillatory flow could be maintained indefinitely by maintaining the required slightly different temperatures on both sides of the junction.

This work was done by Konstantin Penanen and Takso Chui of Caltech for NASA's Jet Propulsion Laboratory. For more information, contact iaoffice@jpl.nasa.gov. NPO-40231

Perturbation Effects on a Supercritical C₇H₁₆/N₂ Mixing Layer

NASA's Jet Propulsion Laboratory, Pasadena, California

A computational-simulation study has been presented of effects of perturbation wavelengths and initial Reynolds numbers on the transition to turbulence of a heptane/nitrogen mixing layer at supercritical pressure. The governing equations for the simulations were the same as those of related prior studies reported in *NASA Tech Briefs*. Two-dimensional (2D) simulations were performed with initially imposed spanwise perturbations whereas three-dimensional (3D) simulations had both streamwise and spanwise initial perturbations.

The 2D simulations were undertaken to ascertain whether perturbations having the shortest unstable wavelength obtained from a linear stability analysis for inviscid flow are unstable in viscous nonlinear flows. The goal of the 3D simulations was to ascertain whether perturbing the mixing layer at different wavelengths affects the transition to turbulence.

It was found that transitions to turbulence can be obtained at different perturbation wavelengths, provided that they are longer than the shortest unsta-

ble wavelength as determined by 2D linear stability analysis for the inviscid case and that the initial Reynolds number is proportionally increased as the wavelength is decreased. The transitional states thus obtained display different dynamic and mixture characteristics, departing strongly from the behaviors of perfect gases and ideal mixtures.

This work was done by Nora Okong'o and Josette Bellan of Caltech for NASA's Jet Propulsion Laboratory. For more information, contact iaoffice@jpl.nasa.gov. NPO-40194

Gold Nanoparticle Labels Amplify Ellipsometric Signals

Marshall Space Flight Center, Alabama

The ellipsometric method reported in the immediately preceding article was developed in conjunction with a method of using gold nanoparticles as labels on biomolecules that one seeks to detect. The purpose of the labeling is to exploit the optical properties of the gold nanoparticles in order to amplify the measurable ellipsometric effects and thereby to enable ultrasensitive detection of the labeled biomolecules without need to develop more-complex ellipsometric instrumentation.

The colorimetric, polarization, light-scattering, and other optical properties of nanoparticles depend on their sizes and shapes. In the present method, these size-

and-shape-dependent properties are used to magnify the polarization of scattered light and the diattenuation and retardance of signals derived from ellipsometry. The size-and-shape-dependent optical properties of the nanoparticles make it possible to interrogate the nanoparticles by use of light of various wavelengths, as appropriate, to optimally detect particles of a specific type at high sensitivity.

Hence, by incorporating gold nanoparticles bound to biomolecules as primary or secondary labels, the performance of ellipsometry as a means of detecting the biomolecules can be improved. The use of gold nanoparticles as labels in ellipsometry has been found to

afford sensitivity that equals or exceeds the sensitivity achieved by use of fluorescence-based methods. Potential applications for ellipsometric detection of gold-nanoparticle-labeled biomolecules include monitoring molecules of interest in biological samples, *in-vitro* diagnostics, process monitoring, general environmental monitoring, and detection of biohazards.

This work was done by Srivatsa Venkatasubbarao of Intelligent Optical Systems, Inc. for Marshall Space Flight Center. For further information, contact Sammy Nabors, MSFC Commercialization Assistance Lead, at sammy.a.nabors@nasa.gov. Refer to MFS-32507-1.

Phase Matching of Diverse Modes in a WGM Resonator

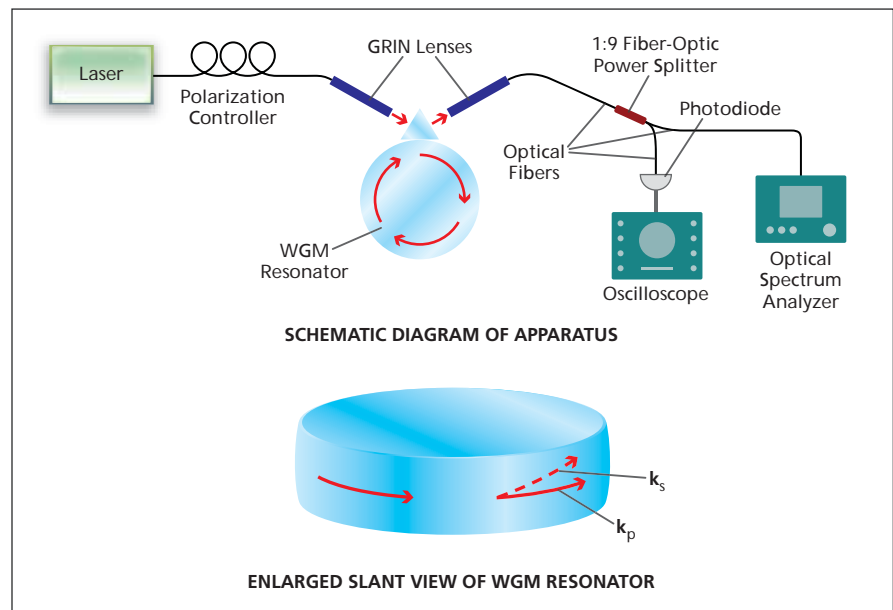
Phase matching is necessary for exploitation of nonlinear optical phenomena.

NASA's Jet Propulsion Laboratory, Pasadena, California

Phase matching of diverse electromagnetic modes (specifically, coexisting optical and microwave modes) in a whispering-gallery-mode (WGM) resonator has been predicted theoretically and verified experimentally. Such phase matching is necessary for storage of microwave/terahertz and optical electromagnetic energy in the same resonator, as needed for exploitation of nonlinear optical phenomena.

WGM resonators are used in research on nonlinear optical phenomena at low optical intensities and as a basis for design and fabrication of novel optical devices. Examples of nonlinear optical phenomena recently demonstrated in WGM resonators include low-threshold Raman lasing, optomechanical oscillations, frequency doubling, and hyperparametric oscillations.

The present findings regarding phase matching were made in research on low-threshold, strongly nondegenerate parametric oscillations in lithium niobate WGM resonators. The principle of operation of such an oscillator is rooted in two previously observed phenomena: (1) stimulated Raman scattering by polaritons in lithium niobate and (2) phase matching of nonlinear optical processes via geometrical confinement of light. The oscillator is



Nonlinear Optical Phenomena are excited in a WGM resonator disk and the output spectrum is measured to obtain evidence of those phenomena. In the phenomenon of particular interest here, an optical pump photon of wave vector k_p is scattered into an optical signal photon of wave vector k_s and a microwave idler photon of wave vector k_i . The idler photon is not necessarily confined within WGM resonator if its wavelength exceeds the thickness of the resonator disk.

partly similar to terahertz oscillators based on lithium niobate crystals, the key difference being that a novel geometrical configuration of this oscillator supports oscillation in the continuous-wave regime. The high resonance quality factors (Q values) typical of WGM

resonators make it possible to achieve oscillation at a threshold signal level much lower than that in a non-WGM-resonator lithium niobate crystal.

The applicable theory states that the parametric interaction takes place in a WGM resonator if the photon-energy

conservation law and the phase-matching condition are satisfied. The photon-energy-conservation law can be stated simply as $\omega_p = \omega_s + \omega_i$, where ω is proportional to the frequency or energy of the photon denoted by its subscript and p, s, and i denote the pump, signal, and idler frequencies, respectively. The phase-matching condition is satisfied if the volume integral of the product of the complex amplitudes of the pump, signal, and idler electromagnetic fields differs from zero.

In the general case, phase matching of an optical field with a microwave field cannot be achieved in a WGM resonator because the indices of refraction of the bulk resonator material are different in the optical and microwave frequency ranges. However, the theory

also shows that it is possible to tailor the spatial structures of the WGM modes, so as to obtain phase matching of fields at resonance frequencies that satisfy the photon-energy-conservation law, through appropriate tailoring of the size and shape of the WGM resonator. This is equivalent to matching of effective indices of refraction for the pump, signal, and idler fields.

Evidence that phase matching can be achieved through suitable choice of size and shape was obtained in experiments on an apparatus depicted schematically in the figure. In each experiment, laser light centered at a wavelength of $\approx 1,319$ nm or $\approx 1,559$ nm was sent through a polarization controller, a grating-index-of-refraction (GRIN) lens, and a diamond prism

into a lithium niobate WGM resonator, and light was coupled out of the WGM resonator through the diamond prism, another GRIN lens, and optical fibers to a photodiode and an optical spectral analyzer. In one experiment, the spectrum of light coming out of the WGM resonator was found to include sidebands associated with strongly nondegenerate parametric oscillations that had been predicted theoretically. In other experiments, oscillations with, variously, confined or unconfined idler fields were observed.

This work was done by Anatoliy Savchenkov, Dmitry Strekalov, Nan Yu, Andrey Matsko, Makan Mohageg, and Lute Maleki of Caltech for NASA's Jet Propulsion Laboratory. Further information is contained in a TSP (see page 1). NPO-45120

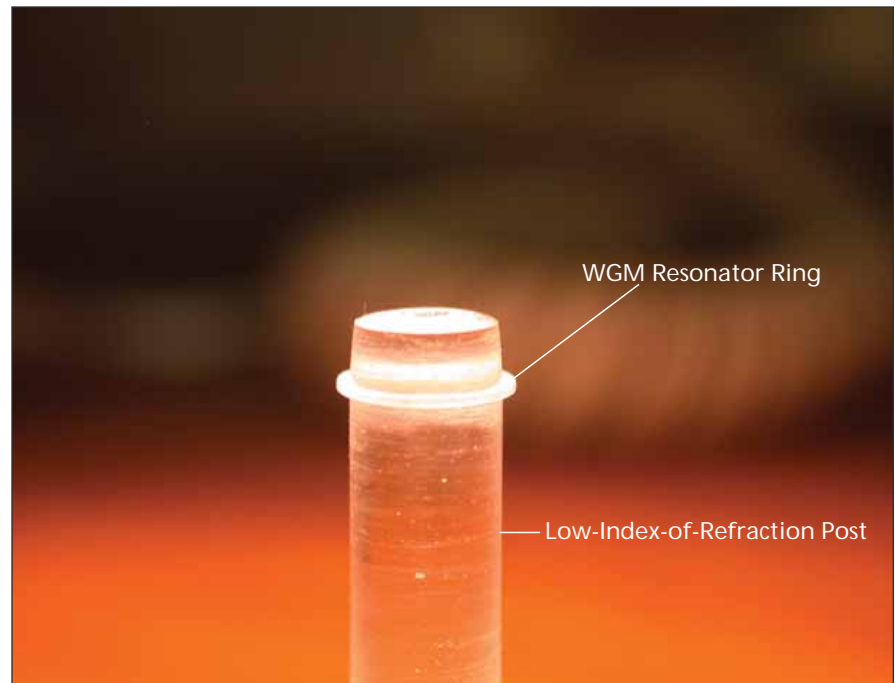
WGM Resonators for Terahertz-to-Optical Frequency Conversion

Receivers containing these devices are contemplated for astronomical and military uses.

NASA's Jet Propulsion Laboratory, Pasadena, California

Progress has been made toward solving some practical problems in the implementation of terahertz-to-optical frequency converters utilizing whispering-gallery-mode (WGM) resonators. Such frequency converters are expected to be essential parts of non-cryogenic terahertz-radiation receivers that are, variously, under development or contemplated for a variety of applications in airborne and spaceborne instrumentation for astronomical and military uses.

In most respects, the basic principles of terahertz-to-optical frequency conversion in WGM resonators are the same as those of microwave (sub-terahertz)-to-optical frequency conversion in WGM resonators, various aspects of which were discussed in the three preceding articles. To recapitulate: In a receiver following this approach, a pre-amplified incoming microwave signal (in the present case, a terahertz signal) is up-converted to an optical signal by a technique that exploits the nonlinearity of the electromagnetic response of a whispering-gallery-mode (WGM) resonator made of LiNbO_3 or another suitable electro-optical material. Up-conversion takes place by three-wave mixing in the resonator. To ensure the required interaction among the optical and terahertz signals, the WGM resonator must be designed and fabricated to function as an electro-optical



A WGM Resonator Ring is mounted on a post made of a material having an index of refraction significantly lower than that of the ring to provide mechanical support without sacrificing confinement of the WGM modes in the ring.

modulator while simultaneously exhibiting (1) resonance at the required microwave and optical operating frequencies and (2) phase matching among the microwave and optical signals circulating in the resonator. Downstream of the WGM res-

onator, the up-converted signal is processed photonically by use of a tunable optical filter or local oscillator and is then detected.

The practical problems addressed in the present development effort are the following:

- Satisfaction of the optical and terahertz resonance-frequency requirement is a straightforward matter, inasmuch as the optical and terahertz spectra can be measured. However, satisfaction of the phase-matching requirement is more difficult. The approach followed in the present development is to perform computer simulations of the microwave and optical signals circulating in the resonator to test for phase matching.
- To enable excitation of the terahertz WGM resonator mode, it is also necessary to ensure phase matching between that mode and the incoming terahertz radiation. In the present

development, the incoming signal is coupled into the WGM resonator via a tapered waveguide in the form of a fused silica rod. The phase-matching requirement is satisfied at one point along the taper; the rod is positioned with this point in proximity to the WGM resonator.

- To maximize the conversion efficiency, it is necessary to maximize the spatial overlap among the terahertz and optical modes in the WGM resonator. In the absence of a special design effort to address this issue, there would be little such overlap because, as a consequence of a

large difference between wavelengths, the optical and terahertz modes would be concentrated at different depths from the rim of a WGM resonator. In the present development, overlap is ensured by constructing the WGM resonator as a ring (see figure) so thin that the optical and terahertz modes are effectively forced to overlap.

This work was done by Dmitry Strelakov, Anatoliy Savchenkov, Andrey Matsko, and Nan Yu of Caltech for NASA's Jet Propulsion Laboratory. Further information is contained in a TSP (see page 1). NPO-45508

⊙ Determining Concentration of Nanoparticles From Ellipsometry

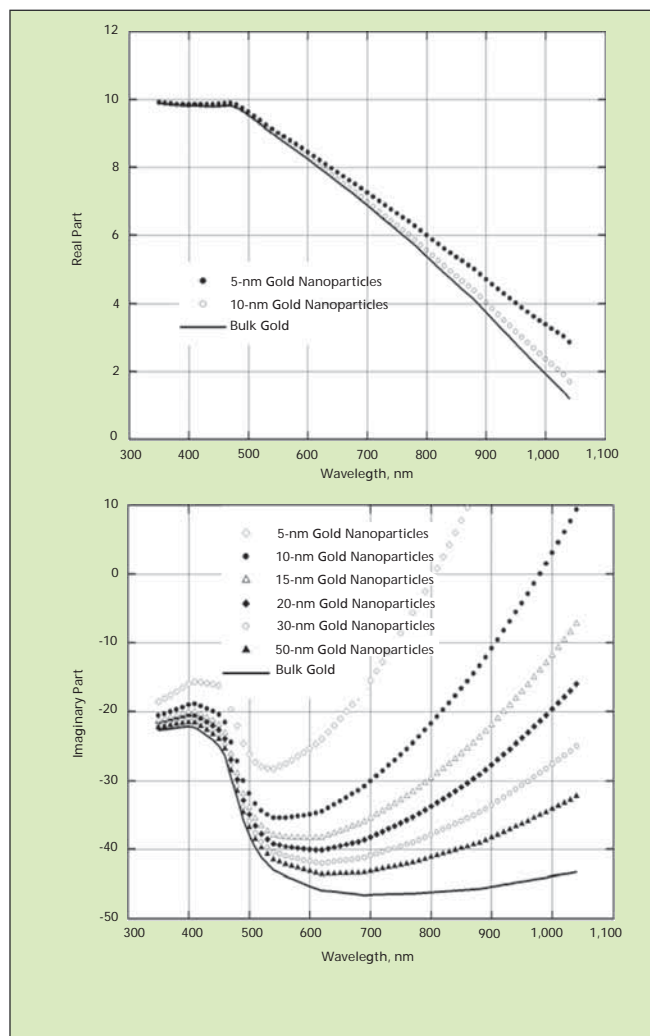
Counting of particles is not necessary.

Marshall Space Flight Center, Alabama

A method of using ellipsometry or polarization analysis of light in total internal reflection of a surface to determine the number density of gold nanoparticles on a smooth substrate has been developed. The method can be modified to enable determination of densities of sparse distributions of nanoparticles in general, and is expected to be especially useful for measuring gold-nanoparticle-labeled biomolecules on microarrays.

The method is based on theoretical calculations of the ellipsometric responses of gold nanoparticles. Elements of the calculations include the following:

- For simplicity, the gold nanoparticles are assumed to be spherical and to have the same radius.
- The distribution of gold nanoparticles is assumed to be a sub-monolayer (that is, sparser than a monolayer).
- The optical response of the sub-monolayer is modeled by use of a thin-island-film theory, according to which the polarizabilities parallel and perpendicular to the substrate are functions of the wavelength of light, the dielectric functions (permit-



Real and Imaginary Parts of complex dielectric functions were determined for bulk gold and for gold nanoparticles having various diameters.

ivities expressed as complex functions of frequency or wavelength) of the gold and the suspending medium (in this case, the suspending medium is air), the fraction of the substrate area covered by the nanoparticles, and the radius of the nanoparticles.

- For the purpose of the thin-island-film theory, the dielectric function of the gold nanoparticles is modeled as the known dielectric function of bulk gold plus a correction term that is necessitated by the fact that the mean free path length for electrons in gold decreases with decreasing radius, in such a manner as to cause the imaginary part of the dielectric function to increase with decreasing radius (see figure). The correction term is a function of the nanoparticle radius, the wavelength of light, the mean free path and the Fermi speed of electrons in bulk gold, the plasma frequency of gold, and the speed of light in a vacuum.

These models are used to calculate ellipsometric responses for various concentrations of gold nanoparticles having an assumed

radius. The modeled data indicates distinct spectral features for both the real and the imaginary part of the dielectric function. An ellipsometric measurement would determine this distinct feature and thus can be used to measure nanoparticle concentration. By “ellipsometric responses” is meant the intensities of light measured in various polarization states as

functions of the angle of incidence and the polarization states of the incident light. These calculated ellipsometric responses are used as calibration curves: Data from subsequent ellipsometric measurements on real specimens are compared with the calibration curves. The concentration of the nanoparticles on a specimen is assumed to be that of the calibration

curve that most closely matches the data pertaining to that specimen.

This work was done by Srivatsa Venkatasubbarao and Lothar U Kempen of Intelligent Optical Systems, Inc. and Russell Chipman of the University of Arizona for Marshall Space Flight Center. For further information, contact Sammy Nabors, MSFC Commercialization Assistance Lead, at sammy.a.nabors@nasa.gov. MFS-32506-1

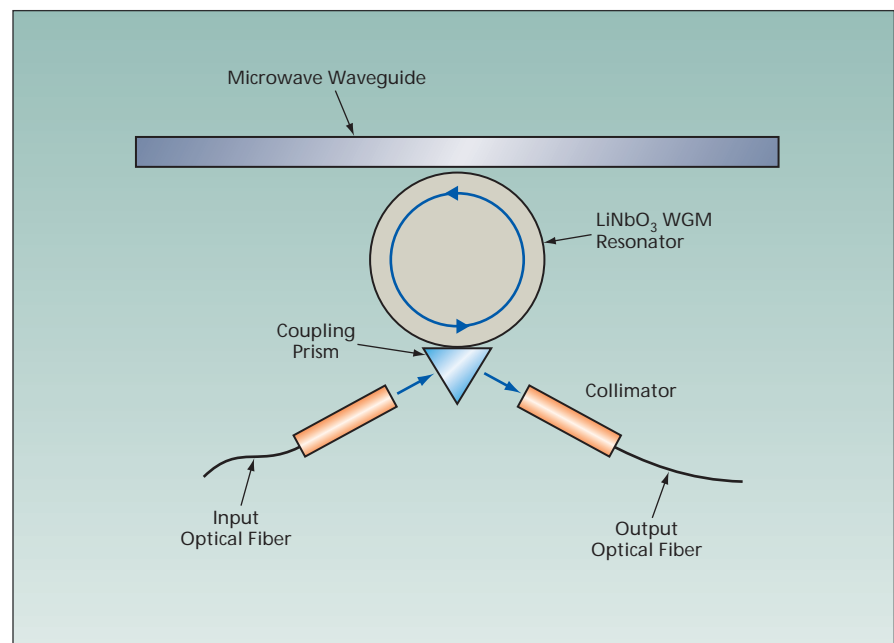
Microwave-to-Optical Conversion in WGM Resonators

Three-wave mixing, resonance, and low loss would result in high efficiency.

NASA's Jet Propulsion Laboratory, Pasadena, California

Microwave-to-optical frequency converters based on whispering-gallery-mode (WGM) resonators have been proposed as mixers for the input ends of microwave receivers in which, downstream of the input ends, signals would be processed photonically. A frequency converter as proposed (see figure) would exploit the nonlinearity of the electromagnetic response of a WGM resonator made of LiNbO_3 or another suitable ferroelectric material. Up-conversion would take place by three-wave mixing in the resonator.

The WGM resonator would be designed and fabricated to obtain (1) resonance at both the microwave and the optical operating frequencies and (2) phase matching among the input and output microwave and optical signals as described in the immediately preceding article. Because the resonator would be all dielectric — there would be no metal electrodes — signal losses would be very low and, consequently, the resonance quality factors (Q values) of the microwave and optical fields would be very large. The long lifetimes associated with the large Q values would enable attainment of high efficiency of nonlinear interaction with low saturation



This Frequency Up-Converter would exploit three-way mixing among a microwave and two optical signals.

power. It is anticipated that efficiency would be especially well enhanced by the combination of optical and microwave resonances in operation at input signal frequencies between 90 and 300 GHz.

This work was done by Anatoliy Savchenkov, Dmitry Strelakov, Nan Yu, Andrey Matsko, and Lute Maleki of Caltech for NASA's Jet Propulsion Laboratory. Further information is contained in a TSP (see page 1). NPO-45121

Four-Pass Coupler for Laser-Diode-Pumped Solid-State Laser

A smaller laser slab can be made to perform comparably to a larger one.

Goddard Space Flight Center, Greenbelt, Maryland

A four-pass optical coupler affords increased (in comparison with related prior two-pass optical couplers) utilization of light generated by a laser diode in side pumping of a solid-state laser

slab. The original application for which this coupler was conceived involves a neodymium-doped yttrium aluminum garnet (Nd:YAG) crystal slab, which, when pumped by a row of laser diodes

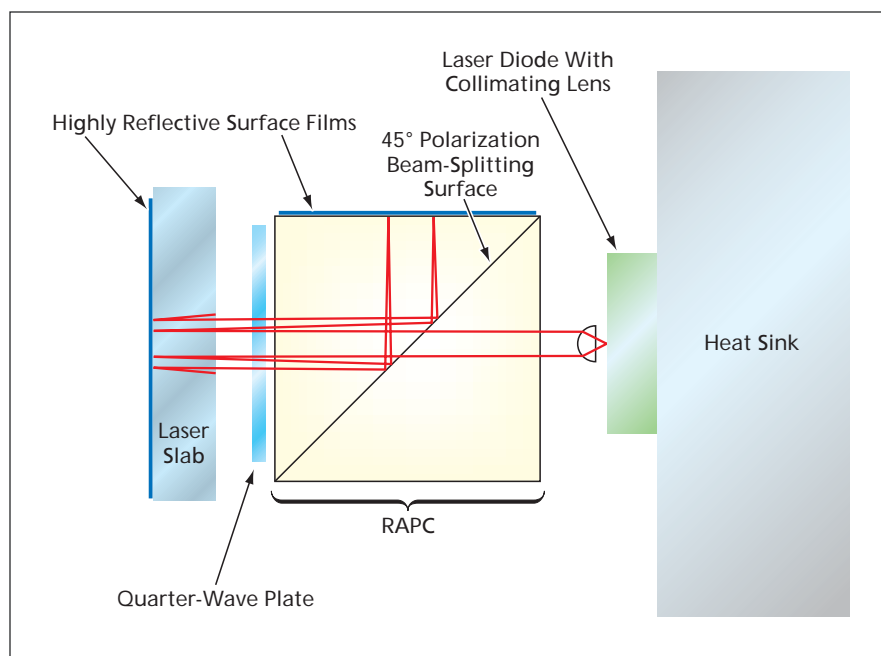
at a wavelength of 809 nm, lases at a wavelength of 1,064 nm.

Heretofore, typically, a thin laser slab has been pumped in two passes, the second pass occurring by virtue of re-

flection of pump light from a highly reflective thin film on the side opposite the side through which the pump light enters. In two-pass pumping, a Nd:YAG slab having a thickness of 2 mm (which is typical) absorbs about 84 percent of the 809-nm pump light power, leaving about 16 percent of the pump light power to travel back toward the laser diodes. This unused power can cause localized heating of the laser diodes, thereby reducing their lifetimes. Moreover, if the slab is thinner than 2 mm, then even more unused power travels back toward the laser diodes.

The four-pass optical coupler captures most of this unused pump light and sends it back to the laser slab for two more passes. As a result, the slab absorbs more pump light, as though it were twice as thick. The gain and laser cavity beam quality of a smaller laser slab in conjunction with this optical coupler can thus be made comparable to those of a larger two-pass-pumped laser slab.

The four-pass coupler (see figure) consists of a right-angle polarization cube (RAPC) with a quarter-wave plate on the side facing the laser slab and highly reflective film coating one of the perpendicular sides. The RAPC transmits p-polarized light (light polarized parallel to the plane of incidence) and reflects s-polarized light (light polarized perpendicular to the plane of incidence). Each laser diode emits a collimated beam and is oriented so that the beam is p-polarized (vertically polarized in the figure). The p-polarized beam passes through the RAPC, and then through the quarter-wave plate, which converts it to a rotationally polarized beam. The beam then passes into the laser slab for



The Four-Pass Coupler is interposed between the laser diodes and the laser slab. This view is along the longitudinal laser axis. The laser diodes, of which only one is shown here, are arranged in a row parallel to the axis.

a first pump pass, reflection, and second pump pass in the usual manner.

The pump light remaining after the second pass leaves the laser slab and travels back into the RAPC via the quarter-wave plate, which converts this light to s polarization. This s-polarized beam is reflected from the internal 45° polarization beam-splitting surface of the RAPC, sending the beam to the reflective coated RAPC surface at normal incidence. After reflection from this surface, this beam is reflected by the 45° surface toward the laser slab and is converted to rotational polarization by the quarter-wave plate. The beam then

makes two more passes through the laser slab in the usual manner.

Any pump beam power remaining after the fourth pass is converted to p polarization by the quarter-wave plate and travels back to the laser diode. However, when the coupler is designed correctly in conjunction with the other laser components, the fraction of pump power returning to the laser diode is too small to exert a significant adverse effect on the laser-diode lifetime or performance.

This work was done by Donald B. Coyle of Goddard Space Flight Center. Further information is contained in a TSP (see page 1). GSC-14961-1

Low-Resolution Raman-Spectroscopy Combustion Thermometry

This method offers advantages over related prior Raman-spectroscopy-based methods.

John H. Glenn Research Center, Cleveland, Ohio

A method of optical thermometry, now undergoing development, involves low-resolution measurement of the spectrum of spontaneous Raman scattering (SRS) from N₂ and O₂ molecules. The method is especially suitable for measuring temperatures in high-pressure combustion environments that contain N₂, O₂, or N₂/O₂ mixtures (including air).

Methods based on SRS (in which scattered light is shifted in wavelength by amounts that depend on vibrational and rotational energy levels of laser-illuminated molecules) have been popular means of probing flames because they are almost the only methods that provide spatially and temporally resolved concentrations and temperatures of multiple molecular species in turbulent

combustion. The present SRS-based method differs from prior SRS-based methods that have various drawbacks, a description of which would exceed the scope of this article. Two main differences between this and prior SRS-based methods are that

- It involves analysis in the frequency (equivalently, wavelength) domain, in contradistinction to analysis in the in-

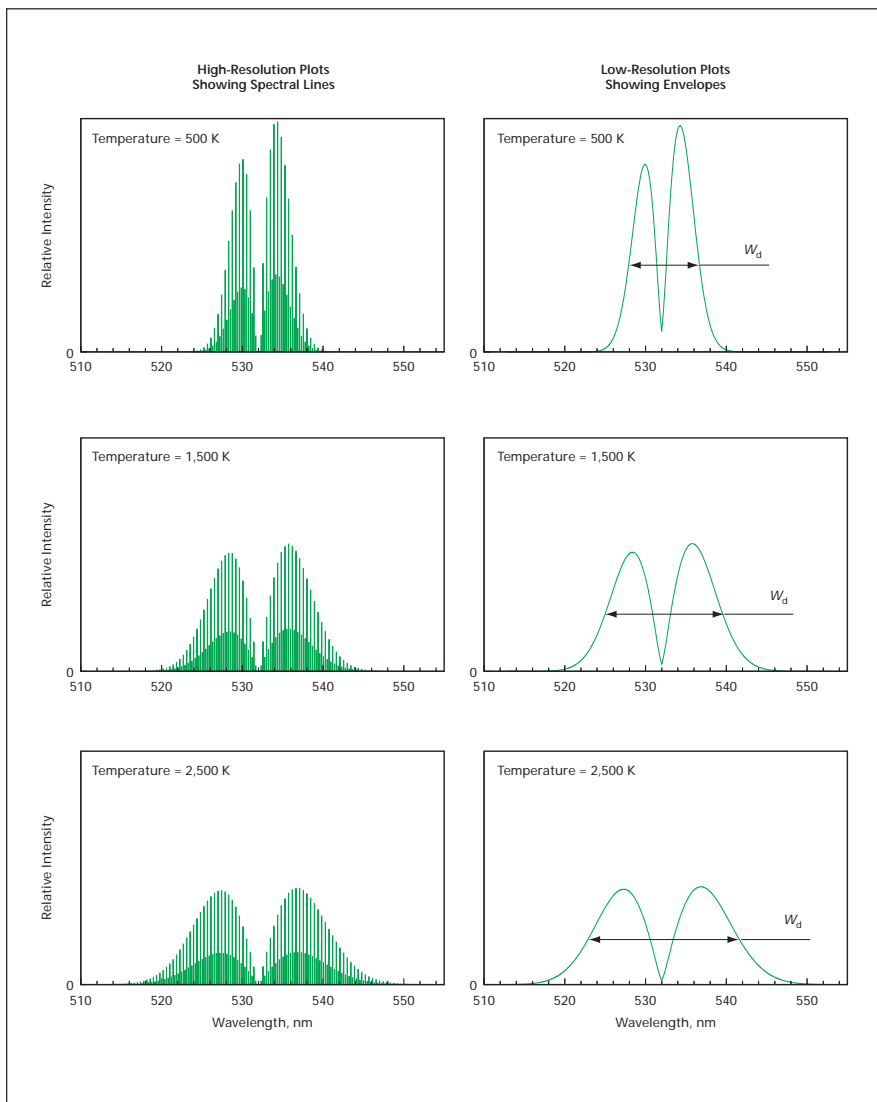


Figure 1. Rotational Raman Spectra of pure N_2 at three temperatures were calculated to show how W_d increases with temperature.

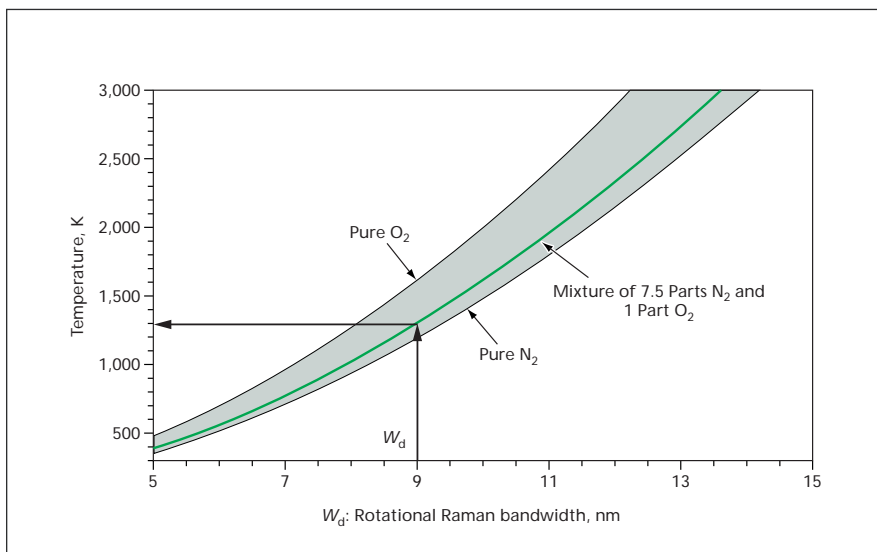


Figure 2. The Conversion Formulas for Pure N_2 and O_2 are represented by the lower and upper boundaries, respectively, of the shaded region. For an N_2/O_2 mixture, the conversion formula lies between these boundaries.

tensity domain in prior methods; and

- It involves low-resolution measurement of what amounts to predominantly the rotational Raman spectra of N_2 and O_2 , in contradistinction to higher-resolution measurement of the vibrational Raman spectrum of N_2 only in prior methods.

Analysis in the frequency domain reduces the effects of uncertainties in the spectral-response calibration and permits greater signal-to-noise ratios by excluding the noise contributed by intensity or amplitude fluctuations. One advantage of utilizing the rotational Raman spectral bands is that they are much stronger than are the vibrational Raman spectral bands. In particular, in this method, one utilizes the rotational N_2 bands near the laser wavelength. The deliberate choice of lower resolution makes it acceptable to use wider spectrograph slits and thereby to collect more light to obtain greater signal-to-noise ratios. A further advantage of lower resolution is the independence of the spectra on pressure broadening effects.

According to theoretical simulations, the rotational Raman spectrum of N_2 widens with increasing temperature (see Figure 1). This is because at higher temperature, greater proportions of rotational states having higher energies become excited. Consequently, it should be possible to establish a relationship between the width W_d of the envelope of the rotational Raman spectrum and the temperature and to express this relationship as a conversion formula for determining the temperature from W_d of a measured spectrum; this is the basic principle of the present method. The method as described thus far would be simple, were it not for the facts that (1) the rotational Raman spectra of N_2 and O_2 overlap and (2) almost any practical combustion system contains N_2 and O_2 . The net effect of the superposition of the N_2 and O_2 rotational Raman spectra is to produce a taller, narrower version of the spectrum of pure N_2 , the amount of narrowing depending on the relative proportions of N_2 and O_2 .

To account for this narrowing, it becomes necessary to generate and use a more comprehensive conversion formula, as illustrated in Figure 2. First, the envelopes of rotational SRS spectra of N_2 and O_2 are calculated theoretically over a range of temperature at a certain pressure to obtain the conversion formulas for N_2 and pure O_2 . Then a blended conversion formula is obtained as a weighted average, wherein the weighting factors

are determined by the relative proportions of N_2 and O_2 as measured or calculated by independent means. (The independent means could be measurements of vibrational Raman spectra of N_2 and O_2 or a chemical-equilibrium calcula-

tion.) Finally, the measured W_d is inserted into the blended conversion formula, yielding the temperature.

This work was done by Quang-Viet Nguyen of Glenn Research Center and Jun Kojima of Ohio Aerospace Institute.

Inquiries concerning rights for the commercial use of this invention should be addressed to NASA Glenn Research Center, Innovative Partnerships Office, Attn: Steve Fedor, Mail Stop 4-8, 21000 Brookpark Road, Cleveland, Ohio 44135. Refer to LEW-18100-1.

Temperature Sensors Based on WGM Optical Resonators

Differences between temperature-dependent frequencies of resonances would be measured.

NASA's Jet Propulsion Laboratory, Pasadena, California

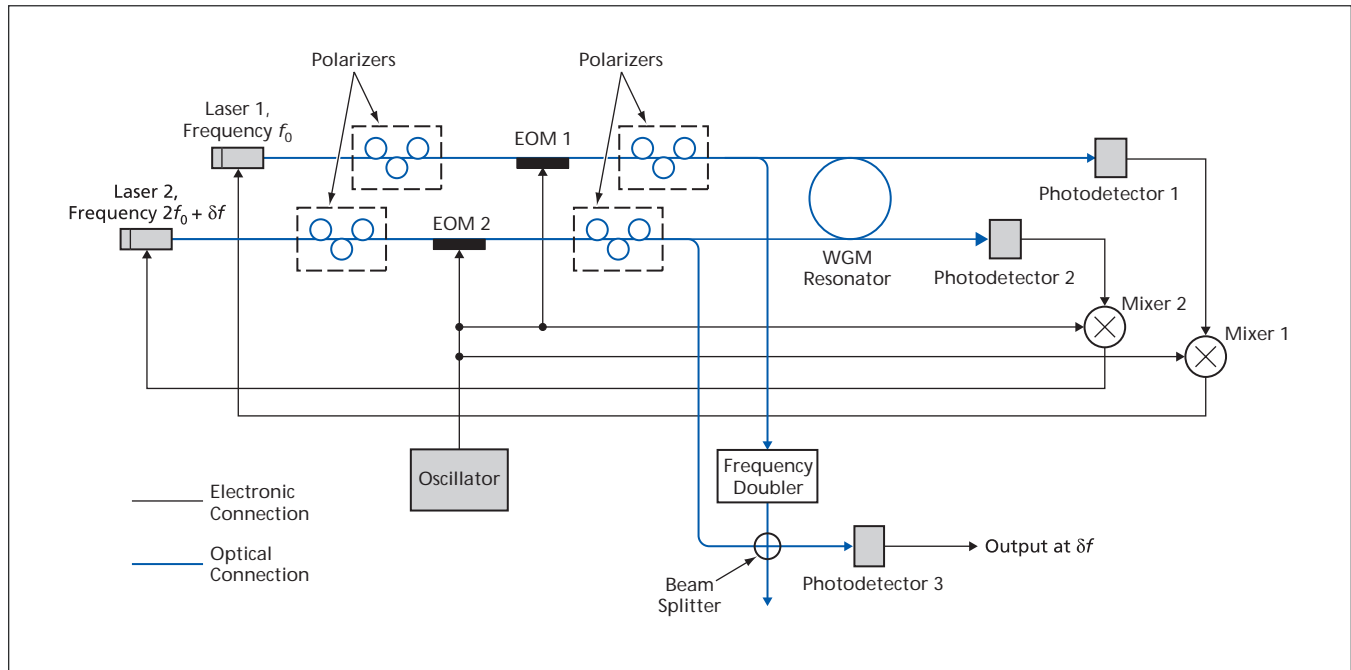
A proposed technique for measuring temperature would exploit differences between the temperature dependences of the frequencies of two different electromagnetic modes of a whispering-gallery-mode (WGM) optical resonator. An apparatus based on this technique was originally intended to be part of a control system for stabilizing a laser frequency in the face of temperature fluctuations. When suitably calibrated, apparatuses based on this technique could also serve as precise temperature sensors for purposes other than stabilization of lasers.

A sensor according to the proposal would include (1) a transparent WGM dielectric resonator having at least two different sets of modes characterized by different thermo-optical constants and (2) optoelectronic instrumentation for measuring the difference between the temperature-dependent shifts of the res-

onance frequencies of the two sets of modes. The figure schematically depicts an example of such a sensor. Laser 1, operating at frequency f_0 , would be locked to a mode in the first of the two sets of WGM modes to be exploited; the mode locking would be accomplished by established means that would include photodetector 1, an oscillator, polarizers, mixer 1, and electro-optical modulator EOM 1. Laser 2, operating at frequency $2f_0 + \delta f$, would be locked to a mode in the second of the two sets of WGM modes to be exploited; in this case, the mode locking would be accomplished by established means that would include photodetector 2, the oscillator, mixer 1, and electro-optical modulator EOM 2.

Part of the modulated output of laser 1 would be fed through a frequency doubler to obtain a modulated beam at frequency $2f_0$. In a beam splitter, the $2f_0$

output from the frequency doubler would be combined with part of the modulated output of laser 2 at $2f_0 + \delta f$. The interference between these combined beams would cause the output of photodetector 3 to include a component at the heterodyne frequency, δf , which would have the desired temperature dependence. Inasmuch as f_0 and δf could readily be chosen to place δf within a suitable radio-frequency range and means for measuring radio frequency precisely are readily available, it would be straightforward to measure δf . Then the temperature could be calculated by inversion of the known temperature dependence of δf . It has been estimated that for a typical CaF_2 WGM resonator having a resonance quality factor (Q) of 2×10^{10} , the temperature-measurement sensitivity would be characterized by a temperature increment of about 40 μK for a frequency increment



The Lasers Would Be Mode-Locked to resonance frequencies f_0 and $2f_0 + \delta f$, respectively, of the WGM resonator. The heterodyne frequency, δf , would vary with temperature and, therefore, would be measured for use as an indication of temperature.

of half the width of one of the resonance spectral peaks.

This work was done by Anatoliy Savchenkov, Nan Yu, Lute Maleki, Vladimir Iltchenko, Andrey Matsko, and Dmitry

Strekalov of Caltech for NASA's Jet Propulsion Laboratory. Further information is contained in a TSP (see page 1).

This invention is owned by NASA, and a patent application has been filed. In-

quiries concerning nonexclusive or exclusive license for its commercial development should be addressed to the Patent Counsel, NASA Management Office-JPL. Refer to NPO-44469.

Varying the Divergence of Multiple Parallel Laser Beams

Lenses mode-matched to the laser beams would be moved axially within an afocal optical subassembly.

NASA's Jet Propulsion Laboratory, Pasadena, California

A provision for controlled variation of the divergence of a laser beam or of multiple parallel laser beams has been incorporated into the design of a conceptual free-space optical-communication station from which the transmitted laser beam(s) would be launched via a telescope. The original purpose to be served by this provision was to enable optimization, under various atmospheric optical conditions, of the divergence of a laser beam or beams transmitted from a ground station to a spacecraft. Beyond the original purpose, the underlying design concept could be beneficial for terrestrial free-space laser communication, ranging, and scientific instrumentation applications in which there are requirements to vary the divergences of laser beams.

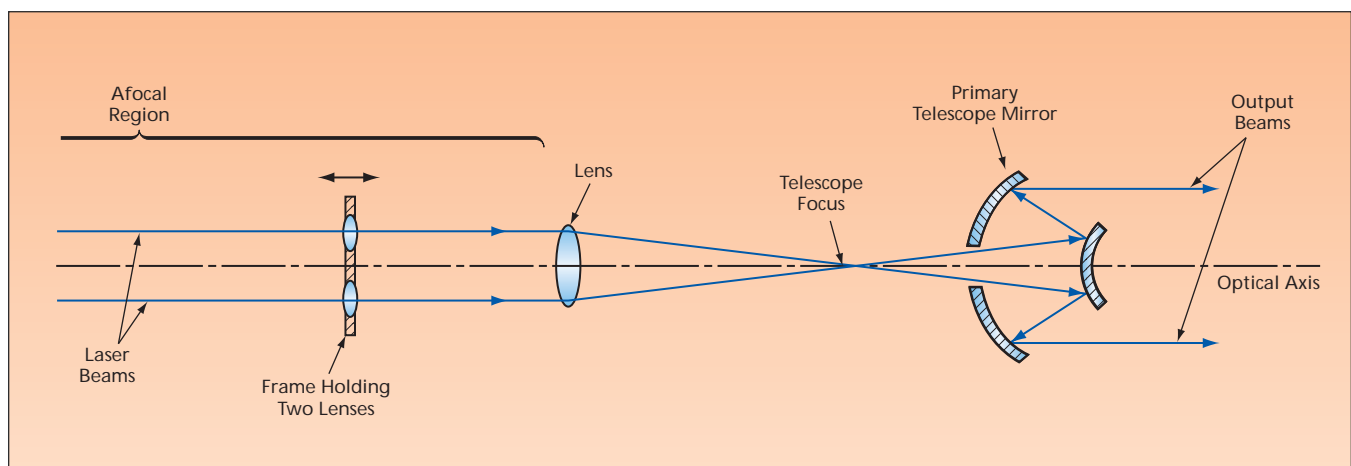
In order to be able to provide for controlled variation of beam divergence, one must first gain detailed understanding of the optical train from each laser to the primary mirror of the telescope. Gaussian propagation of each laser

beam through all the optical elements must be computed. If multiple parallel beams were to be transmitted, then by means of previously developed optics, they would be positioned symmetrically about the optical axis. It would be necessary to perform paraxial ray tracing to ensure that the beams emerging from the primary mirror into free space were parallel to each other and to the main optical axis of the telescope.

The design concept reflects a requirement in the original application that final divergence of the beam(s) propagating out from the primary mirror into free space be varied by moving only one lens or lens assembly in the optical train and that this motion not cause the outgoing beam(s) to deviate from parallelism with the optical axis. To satisfy this requirement, the telescope would incorporate an afocal optical subassembly, within which either a single on-axis lens in the case of a single laser beam or a ring assembly of

lenses in the case of multiple laser beams (see figure) would be moved. The lens or lenses must be designed to mode-match the laser output through the afocal subassembly and telescope optics to produce the required beam divergence. By moving this lens (or moving the assembly of lenses as a single unit) along the optical axis, one would cause the divergence of the outgoing laser beam(s) to vary through the required range. Care must be taken to ensure that there is no apodization or vignetting through any limiting apertures in the overall optical system and that power density of any laser beam must not be so high as to result in dielectric breakdown of air or in damage to any optic along the optical path.

This work was done by Joseph M. Kovalik and Malcolm W. Wright of Caltech for NASA's Jet Propulsion Laboratory. For more information, contact iaoffice@jpl.nasa.gov. NPO-43967



A Frame Would Hold Lenses placed symmetrically about the optical axis to intercept multiple laser beams parallel to the axis. (For simplicity, only two beams are shown here, but the original design calls for eight beams). The frame would be moved along the optical axis to vary the divergence of the laser beams emerging from the primary telescope mirror. The motion of the frame and lenses would not cause the beams to deviate from parallelism with the optical axis.



Efficient Algorithm for Rectangular Spiral Search

The search pattern is automatically expanded as needed.

NASA's Jet Propulsion Laboratory, Pasadena, California

An algorithm generates grid coordinates for a computationally efficient spiral search pattern covering an uncertain rectangular area spanned by a coordinate grid. The algorithm does not require that the grid be fixed; the algorithm can search indefinitely, expanding the grid and spiral, as needed, until the target of the search is found. The algorithm also does not require memory of coordinates of previous points on the spiral to generate the current point on the spiral.

The search is started at a point (more precisely, in a grid cell), denoted the center of the spiral, that has been chosen previously as the point most likely to coincide with the target. The search is to be performed on a grid of $m \times n$ cells, where $m > n$ and $a \equiv m - n$ is denoted the

rectangular excess of the search pattern (see Figure 1). The spiral search is performed in steps numbered simply 1, 2, 3..., and t represents the number of the current step.

The inputs to the algorithm are t and the rectangular excess that is either specified in advance or calculated from the rectangular grid used to span the initial search area. The output of the algorithm is the pair of integer coordinates (i,j) of the current point on the spiral with respect to the center of

the spiral. Figure 2 presents, as an example, the first 15 steps of the spiral generated by this algorithm for a search that starts at a point in a 3×5 rectangle.

This work was done by Paul Brugarolas and William Breckenridge of Caltech for NASA's Jet Propulsion Laboratory.

The software used in this innovation is available for commercial licensing. Please contact Karina Edmonds of the California Institute of Technology at (626) 395-2322. Refer to NPO-42057.

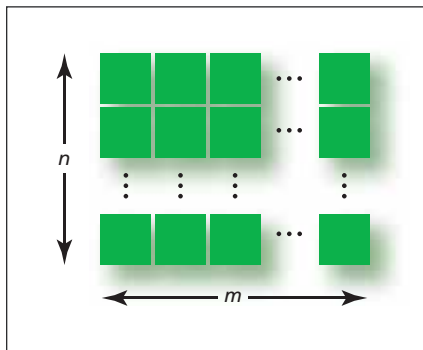


Figure 1. A Rectangular Grid of $n \times m$ cells is overlaid on the area to be searched.

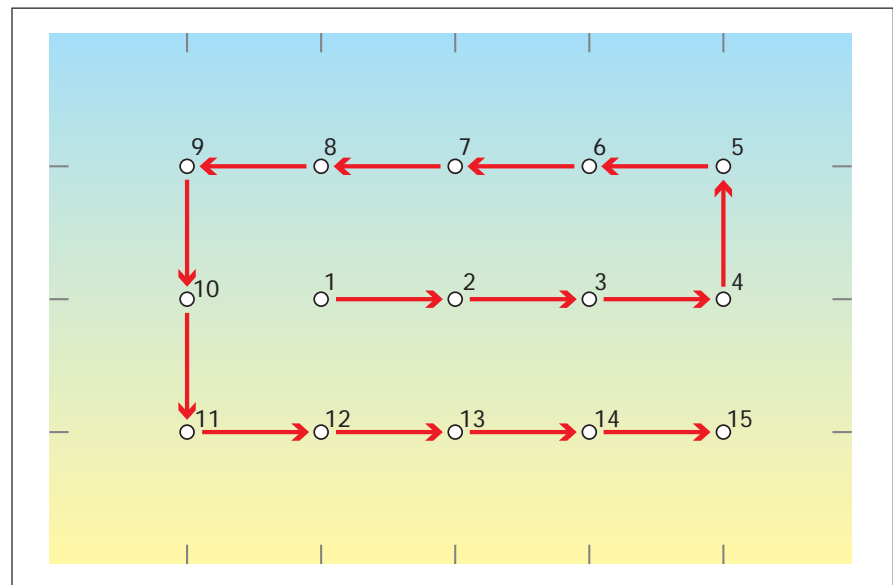


Figure 2. A Spiral Search Pattern was generated in an area initially overlaid with a 3×5 grid.

Algorithm-Based Fault Tolerance Integrated With Replication

NASA's Jet Propulsion Laboratory, Pasadena, California

In a proposed approach to programming and utilization of commercial off-the-shelf computing equipment, a combination of algorithm-based fault tolerance (ABFT) and replication would be utilized to obtain high degrees of fault tolerance without incurring excessive costs. The basic idea of the proposed approach is to integrate ABFT with replication such that the algorithmic portions of computations

would be protected by ABFT, and the logical portions by replication.

ABFT is an extremely efficient, inexpensive, high-coverage technique for detecting and mitigating faults in computer systems used for algorithmic computations, but does not protect against errors in logical operations surrounding algorithms. Replication is a generally applicable, high-coverage technique for protecting general com-

putations from faults, but is inefficient and costly because it requires additional computation time or additional computational circuitry (and, hence, additional mass and power). The goal of the proposed integration of ABFT with replication is to optimize the fault-tolerance aspect of the design of a computing system by using the less-efficient, more-expensive technique to protect only those computations that cannot be protected

by the more-efficient, less-expensive technique. It would not be necessary to address the fault-tolerance issue explicitly in writing an application program to be executed in such a system. Instead,

ABFT and replication would be managed by middleware containing hooks.

This work was done by Raphael Some and David Rennels of Caltech for NASA's Jet Propulsion Laboratory.

The software used in this innovation is available for commercial licensing. Please contact Karina Edmonds of the California Institute of Technology at (626) 395-2322. Refer to NPO-43842.

➤ Targeting and Localization for Mars Rover Operations

NASA's Jet Propulsion Laboratory, Pasadena, California

A design and a partially developed application framework were presented for improving localization and targeting for surface spacecraft. The program has value for the Mars Science Laboratory mission, and has been delivered to support the Mars Exploration Rovers as part of the latest version of the Maestro science planning tool. It also has applications for future missions involving either surface-based or low-altitude atmospheric robotic vehicles.

The targeting and localization solutions solve the problem of how to integrate localization estimate updates into

operational planning tools, operational data product generalizations, and flight software by adding expanded flexibility to flight software, the operations data product pipeline, and operations planning tools based on coordinate frame updates during a planning cycle. When acquiring points of interest (targets) for the rover, instead of using a temporal method for reusing previously acquired targets, this system uses a spatial method to avoid tedious and repetitive target re-designation needed to keep target relevance accurate. Instead of creating a target that is reusable only

for a sol (Martian day), the target is defined in a way to make it reusable for a planning position (the vehicle position indicated by a Site and Drive index pair) from which the vehicle will begin a command cycle.

This work was done by Mark W. Powell, Thomas Crockett, Jason M. Fox, Joseph C. Joswig, Jeffrey S. Norris, and Kenneth J. Rabe of NASA's Jet Propulsion Laboratory.

The software used in this innovation is available for commercial licensing. Please contact Karina Edmonds of the California Institute of Technology at (626) 395-2322. Refer to NPO-43847.

➤ Terrain-Adaptive Navigation Architecture

NASA's Jet Propulsion Laboratory, Pasadena, California

A navigation system designed for a Mars rover has been designed to deal with rough terrain and/or potential slip when evaluating and executing paths. The system also can be used for any off-road, autonomous vehicles. The system uses more sophisticated terrain analysis, but also converges to computational complexity similar to that of currently deployed navigation systems when the terrain is benign. The system consists of technologies that have been developed, integrated, and

tested onboard research rovers in Mars analog terrains, including goodness maps and terrain triage, terrain classification, remote slip prediction, path planning, high-fidelity traversability analysis (HFTA), and slip-compensated path following.

The system enables vehicles to autonomously navigate different terrain challenges including dry river channel systems, putative shorelines, and gullies emanating from canyon walls. Several of the technologies within this innovation

increase the navigation system's capabilities compared to earlier rover navigation algorithms.

This work was done by Daniel M. Helmick, Anelia Angelova, Larry H. Matthies, and Daniel M. Helmick of Caltech for NASA's Jet Propulsion Laboratory.

The software used in this innovation is available for commercial licensing. Please contact Karina Edmonds of the California Institute of Technology at (626) 395-2322. Refer to NPO-44588.

➤ Self-Adjusting Hash Tables for Embedded Flight Applications

NASA's Jet Propulsion Laboratory, Pasadena, California

A common practice in computer science to associate a value with a key is to use a class of algorithms called a hash-table. These algorithms enable rapid storage and retrieval of values based upon a key. This approach assumes that many keys will need to be stored immediately. A new set of hash-table algorithms optimally uses system resources to ideally represent keys and

values in memory such that the information can be stored and retrieved with a minimal amount of time and space. These hash-tables support the efficient addition of new entries. Also, for large data sets, the look-up time for large data-set searches is independent of the number of items stored, i.e., $O(1)$, provided that the chance of collision is low.

Like arrays, hash-tables provide constant time $O(1)$ look-up on average, regardless of the number of items in the table. However, the rare worst-case look-up time can be as bad as $O(n)$. Compared to other associative array data structures, hash-tables are most useful when large numbers of records are to be stored, especially if the size of the data set can be predicted.

These algorithms may be used as in-memory data structures and may also be adopted for use with persistent data structures. Hash-tables are used in thousands of instances of flight code, and this approach could improve the efficiency of those applications, allowing them to run in smaller memory footprints and to autonomously evolve with time if and

when their data demands a more efficient representation.

This work was done by Mark James of Caltech for NASA's Jet Propulsion Laboratory. Further information is contained in a TSP (see page 1).

In accordance with Public Law 96-517, the contractor has elected to retain title to this invention. Inquiries concerning rights for its

commercial use should be addressed to:

*Innovative Technology Assets Management
JPL*

Mail Stop 202-233

4800 Oak Grove Drive

Pasadena, CA 91109-8099

E-mail: iaoffice@jpl.nasa.gov

Refer to NPO-40363, volume and number of this NASA Tech Briefs issue, and the page number.

Schema for Spacecraft-Command Dictionary

NASA's Jet Propulsion Laboratory, Pasadena, California

An Extensible Markup Language (XML) schema was developed as a means of defining and describing a structure for capturing spacecraft command-definition and tracking information in a single location in a form readable by both engineers and software used to generate software for flight and ground systems. A structure defined within this schema is then used as the basis for creating an XML file that contains command definitions. The schema is divided into three sections:

- Header information, including infor-

mation about the project and XML file to be derived from the schema;

- Project-specific definitions of types, roles, and allowable values of data; and
- The information necessary for defining the command structure, including the information necessary for generating all pertinent software.

Among the advantages afforded by XML for such applications are the following:

- There exist commercial off-the-shelf (COTS) software tools and standard scripting-language modules for pars-

ing XML schemata. These tools and modules facilitate the ingestion of XML files for use.

- By use of COTS software tools, the structures of, and some properties of the data in, XML files can be validated against their parent XML schemata to detect errors early.

*This work was done by Sharon Laubach, Celina Garcia, Scott Maxwell, and Jesse Wright of Caltech for NASA's Jet Propulsion Laboratory. For more information, contact iaoffice@jpl.nasa.gov.
NPO-42332*



Books & Reports

Combined GMSK Communications and PN Ranging

A document discusses a method by which GMSK (Gaussian minimum shift keying) modulation and a pseudonoise (PN) ranging signal may be combined. By isolating the in-phase and quadrature components after carrier lock, and extracting their low-pass and band-pass filtered components, there is enough information available to both demodulate data and track the PN signal. The proposed combined GMSK communications and PN ranging is one potential approach to address emerging requirements for simultaneous high data rate communications from and tracking of vehicles in deep space or at the Moon.

GMSK and PN ranging have not been previously combined, and the corresponding receiver structure for such combined ranging has not been proposed in the past. A key advantage is that the combined signal is bandwidth-efficient and it is a constant envelope modulation, allowing high-power amplifiers to operate at saturation for highest efficiency.

This work was done by Richard Orr of SATEL LLC and Dariush Divsalar of Caltech for NASA's Jet Propulsion Laboratory. Further information is contained in a TSP (see page 1). NPO-45108

System-Level Integration of Mass Memory

A report discusses integrating multiple memory modules on the high-speed serial interconnect (IEEE 1393) that is used by a spacecraft's inter-module communications in order to ease data congestion and provide for a scalable, strong, flexible system that can meet new system-level mass memory requirements.

Using the JPL 1393 Ring Bus Interconnect to link computer elements, I/O, and memory allows any element to communicate with any other element. Besides providing a consistent approach to exchanging data, it inherently has a layer of abstraction that allows for better system and software design. This new architecture is fault-tolerant and provides a large range of scalability while supporting flexible spacecraft architectures that are currently being investigated.

This work was done by Brian Cox, Jeffrey Mellstrom, and Terry Wysocky of Caltech

for NASA's Jet Propulsion Laboratory. Further information is contained in a TSP (see page 1).

In accordance with Public Law 96-517, the contractor has elected to retain title to this invention. Inquiries concerning rights for its commercial use should be addressed to:

*Innovative Technology Assets Management
JPL*

Mail Stop 202-233

4800 Oak Grove Drive

Pasadena, CA 91109-8099

E-mail: iaoffice@jpl.nasa.gov

Refer to NPO-45205, volume and number of this NASA Tech Briefs issue, and the page number.

Network-Attached Solid-State Recorder Architecture

A document discusses placing memory modules on the high-speed serial interconnect, which is used by a spacecraft's computer elements for inter-processor communications, to allow all multiple computer system architectures to access the spacecraft data storage at the same time. Each memory board is identical electrically and receives its bus ID upon connection to the system. The computer elements are configured in a similar fashion. The architecture allows for multiple memory boards to be accessed simultaneously by different computer elements, and results in a scalable, strong, fault-tolerant system. The IEEE-1393 ring bus can be routed so that multiple card failures can occur and the mass memory storage will still function.

This work was done by Brian Cox of Caltech for NASA's Jet Propulsion Laboratory. Further information is contained in a TSP (see page 1). NPO-45204

Method of Cross-Linking Aerogels Using a One-Pot Reaction Scheme

A document discusses a new, simplified method for cross-linking silica and other oxide aerogels, with a polymeric material to increase strength of such materials without adversely affecting porosity or low density. The usual process is long and arduous, requiring multiple washing and soaking steps to infiltrate oxide with the polymer precursor after gelation. Additionally, diffusion prob-

lems can result in aerogel monoliths that are not uniformly cross-linked.

This innovation introduces the polymer precursor into the sol before gelation either as an agent, which co-reacts with the oxide gel, or as soluble polymer precursors, which do not interact with the oxide gel in any way. Subsequent exposure to heat, light, catalyst or other method of promoting polymerization causes cross-linking without any additional infiltration steps.

The resulting aerogel monolith is more uniform because this process does not suffer from diffusion issues that previous methods have. Also, in instances where complete polymerization requires a balanced stoichiometry, this requirement is more easily met.

This work was done by Mary Ann B. Meador and Lynn A. Capadona of Glenn Research Center. Further information is contained in a TSP (see page 1).

Inquiries concerning rights for the commercial use of this invention should be addressed to NASA Glenn Research Center, Innovative Partnerships Office, Attn: Steve Fedor, Mail Stop 4-8, 21000 Brookpark Road, Cleveland, Ohio 44135. Refer to LEW-18042.

An Efficient Reachability Analysis Algorithm

A document discusses a new algorithm for generating higher-order dependencies for diagnostic and sensor placement analysis when a system is described with a causal modeling framework. This innovation will be used in diagnostic and sensor optimization and analysis tools. Fault detection, diagnosis, and prognosis are essential tasks in the operation of autonomous spacecraft, instruments, and *in-situ* platforms. This algorithm will serve as a power tool for technologies that satisfy a key requirement of autonomous spacecraft, including science instruments and *in-situ* missions.

In the causal modeling, the system is modeled in terms of first-order cause-and-effect dependencies; i.e., how the fault propagates from a faulty component to its immediate neighbors. For diagnostic purpose, also global (or higher-order) dependencies are needed, which is the effect of a fault on non-neighbor components. The global dependencies should be inferred from the first-order

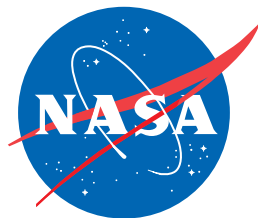
dependencies. The method that finds these dependencies is called a reachability analysis algorithm. The result of this algorithm determines at each test point (or sensor position) which of the failure sources can be observed.

The standard reachability analysis algorithm uses a “token propagation” method. The complexity of this algo-

rithm is proportional to the product EN , where E is the number of links (edges) of the graph of the system and N is the number of components. Here a new algorithm is introduced. The complexity of this algorithm is proportional to the product dN , where d is the length of the longest (directed) path in the graph of the system. To compare the perform-

ance of these two algorithms, first it is noted that always $d \leq E$. But typically, d is of the order of $\log(E)$; thus the new algorithm, in general, outperforms the standard algorithm.

This work was done by Farrokh Vatan and Amir Fijany of Caltech for NASA's Jet Propulsion Laboratory. Further information is contained in a TSP (see page 1). NPO-45797



National Aeronautics and
Space Administration